

Accurate experimental benchmark study of a catamaran in regular and irregular head waves including uncertainty quantification

D. Durante ^{a,*}, R. Broglia ^a, M. Diez ^a, A. Olivieri ^a, E.F. Campana ^a, F. Stern ^b

^a CNR-INM, National Research Council - Institute of Marine Engineering, Rome, Italy

^b IHR-Hydroscience and Engineering, The University of Iowa, Iowa City, IA, USA

ARTICLE INFO

Keywords:

EFD
Seakeeping
Regular and irregular waves
Uncertainty quantification
Subseries method
Bootstrap method
Validation
Delft catamaran

ABSTRACT

Irregular wave experiments are essential to assess the statistics of ship responses in realistic operating conditions and to validate the associated numerical simulations. The cost and time required to achieve statistically-converged results are usually high (both experimentally and computationally). For these reasons, high-quality statistically-converged irregular wave studies are limited in the literature and models to reduce the experimental/computational costs are highly desirable. Here, a statistically-converged experimental benchmark study of a catamaran in irregular waves is presented, along with regular-wave Uncertainty Quantification (UQ) model used to approximate the relevant statistical estimators. The statistical assessment is achieved through recently-developed approaches based on the analysis of the autocovariance function of the ship response, along with block-bootstrap and bootstrap methods. The validation variables are the wave elevation, axial force, heave and pitch motions, vertical acceleration of the bridge and vertical velocity of the flight-deck. Values from the time series are addressed as primary variables, whereas heights associated to mean-crossing waves are referred to as secondary variables. The statistical uncertainty related to Expected Value (EV) and Standard Deviation (SD) of primary variables is evaluated through autocovariance analysis and block-bootstrap methods. The latter are used to assess also the quantile function. EV, SD, and quantile function of secondary variables are then assessed by the bootstrap method. Regular-wave models assess the EV of the axial force, and single significant amplitudes (twice the SD) of pitch, acceleration, and velocity, as relevant merit factors used for design optimization in earlier studies.

1. Introduction

In ship design it is important to predict the behavior of a floating structure when it is subjected to waves. Seakeeping directly impacts the design of a vessel and, for this reason, the transfer functions (i.e. the so-called Response Amplitude Operators, RAO) should be calculated for all six motions and for all relative wave headings. However, in real-world applications all the relevant outputs are affected by uncertainty. This stems from operational and environmental parameters, as well as geometrical tolerances and numerical/modeling errors. The estimate of the output uncertainty is required in order to provide the suitable confidence intervals of the relevant parameters. Uncertainty studies moved from deterministic Uncertainty Analysis (UA) for verification and validation (V&V) for numerical and modeling errors (Stern et al. (2001), (Stern et al., 2006); Xing and Stern (2010)) to stochastic Uncertainty Quantification (UQ) for environmental and operating conditions. Earlier

research addressed Reynolds averaged Navier-Stokes (RANS) based simulations of a NACA0012 hydrofoil with variable Reynolds number (Mousaviraad et al. (2013a)), unsteady RANS and potential flow simulations of the Delft catamaran in calm water with variable Froude number (Fr) and geometry (Diez et al. (2014)), and unsteady RANS simulations of a high-speed catamaran in irregular and stochastic regular waves, with variable geometry (He et al. (2013); Diez et al. (2013)).

The 24th International Towing Tank Conference (ITTC, 2005) has identified several drawbacks of the current database for seakeeping experiments:

- the Series 60 or S-175 container are the most considered in seakeeping studies as test geometries
- the head seas conditions are usually preferred
- focus on small steepness conditions in the linear regime
- do not provide body plan, offsets, or loading weight distributions

* Corresponding author.

E-mail address: danielo.durante@cnr.it (D. Durante).

- partially or do not report UA procedures and uncertainties.

As a result, very few seakeeping experimental fluid dynamics (EFD) information exist that may be useful as benchmark data for validation of computational fluid dynamics (CFD) seakeeping codes. Longo and Stern (2005) and Stern et al. (2006) provide data sets of typical towing tank tests and the methodology for computing and reporting the UA results of the measurement variables.

The Delft catamaran is an international benchmark geometry, which has been used for CFD and EFD studies. Earlier research on the Delft catamaran includes seakeeping CFD (Castiglione et al. (2011)) and EFD (Bouscasse et al. (2013)), steady drift CFD (Broglia et al. (2015) and (Broglia et al., 2019; Huang et al., 2008) and EFD (Falchi et al. (2014)) for the onset and progression of vortices, CFD (Castiglione et al. (2014); He et al (He et al., 2015).) and EFD (Broglia et al. (2014)) interference factor studies, and CFD water-jet/maneuvering studies (Sadat-Hosseini et al. (2013)), and deterministic design optimization (Chen et al. (2013), (Chen et al., 2015); Diez et al. (2015b)). However, experimental UQ studies and validation of UQ methods for the irregular wave statistics are still lacking.

Stochastic UQ methods and approximations are an essential part of stochastic simulation-based design optimization (such as reliability-based and robust design optimization) for real ocean environment and operations. Diez et al. (2013)), and Tahara et al. (2014) presented a multi-objective design optimization for resistance and operability in real ocean environment and operations (including variable sea state and speed, but limited to head waves) for the Delft catamaran. The approach encompasses a single deterministic regular wave approximation for the evaluation of the mean resistance in wave and a stochastic regular wave UQ model for the single significant amplitudes (SSAs) of the relevant constrained variables (pitch, acceleration of bridge, and velocity of flight deck, as per the NATO standardization agreement STANAG 4154, e.g., Kennell et al. (1985) and NATO (NATO STANAG 4154, 1997)). The results from the approximated deterministic and stochastic regular wave UQ models compared well with numerical benchmark values, based on irregular wave simulation.

The objective of the present work is the experimental validation of UQ methods developed and applied in earlier studies for design optimization. The focus is on the (a) irregular wave benchmark analysis, and (b) stochastic regular wave UQ model, along with the assessment of the validation methods and comparison of the resulting confidence intervals.

The approach includes experiments in irregular waves (taken as experimental benchmark) followed by regular wave UQ. The validation variables are the wave elevation ζ , x-force, heave z , pitch θ , vertical acceleration of the bridge \ddot{z}_B and the vertical velocity of the flight deck \dot{z}_D . The current approach addresses the statistics of the irregular wave time series as primary variables and mean-crossing amplitudes as secondary variables, providing their expected value (EV), standard deviation (SD) and cumulative/probability density functions (CDF/PDF). The subseries (Carlstein (1986),) and bootstrap (Efron (1981),) methods give the required validation values and confidence intervals for EV, SD and CDF (expressed by the quantile function) of primary and secondary variables, respectively. The combined use of the kernel density estimator, KDE, (Miecznikowski et al. (2010a)) with the subseries and bootstrap methods provides validation values and confidence intervals for the PDF. Additionally, validation values and confidence intervals of time series EV and SD are evaluated using the sample variance and size, and the autocovariance function, as shown by Belenky et al. (2015). The regular wave UQ focuses on EV of axial force and SSAs of pitch motion, acceleration and velocity, as relevant merit factors for design optimization. The model tests are conducted at CNR-INM.

Recently, CFD versus EFD validation studies for irregular waves of high speed planning crafts were presented by Mousaviraad et al. (2013b), Fu et al. (2014) and Diez et al. (2018b). Similarly to the current work, Sadat-Hosseini et al. (2015) show CFD versus EFD validation

studies of irregular waves for the 5415M model, including a comparison of unsteady RANS and potential flow solutions with experimental data, and showing the effects of the number of inlet wave components on the validation errors.

The present paper is organized as follows: in Section 2, an overview of the experimental setup, with a presentation of the instrumentation used, is given; in Section 3, statistical estimators and confidence intervals for regular and irregular waves are indicated; in Section 4, the results of the experiments in irregular and in regular waves are outlined together with their uncertainty analysis and finally compared. In Section 5, conclusions are offered.

2. Experimental setup

In this section experimental setup is described in details. The catamaran model is shown in section 2.1; in order to measure motions and longitudinal force the vessel is completely instrumented, whereas, the towing carriage is equipped for the wave height measurements. Instrumentations and the facility are illustrated in sections 2.2 and 2.3. It has to be highlighted that a carefully assessment of the wave generation and propagation has been pursued, being mandatory for the high fidelity measurements required for a valuable UQ analysis.

2.1. Catamaran model

The TU Delft-372 catamaran (Van't Veer (Van't Veer, 1998a), (Van't Veer, 1998b)) has been selected as a case study for the current benchmark. A fiberglass model was manufactured (CNR-INM model 2554) at the same scale of the Delft one (i.e. $L_{pp} = 3m$). A full scale vessel has never been built, anyhow, in order to properly select the operative condition in a real scenario, a 100m catamaran at full scale (i.e. a $\lambda = 33.33$ scale factor) has been considered in the following.

The basic geometry and the body plan of the model are sketched in Fig. 1, the CNR-INM 2554 model is shown in Fig. 2; the main geometric, hydrostatic and hydrodynamic properties at model and full scales are given in Table 1.

The model is towed through a twin-gimbal (one for each demi-hull) rigidly connected with a transversal beam which ensures free pitch motion around the center of gravity, and a vertical beam sliding in a linear bearing which allows free heave motion. The linking system ensures that surge, sway and roll are so restricted that they may be assumed as restrained. Yaw is kept fixed by means of a motion preventer. To increase the rigidity of the catamaran model, the two demi-hulls are connected with two transversal aluminum beams ahead and behind the center of gravity and a third aluminum beam at the aft perpendicular as shown in Fig. 2. The configuration ensures enough rigidity of the catamaran without using a deck in the fore part of the model; therefore, no

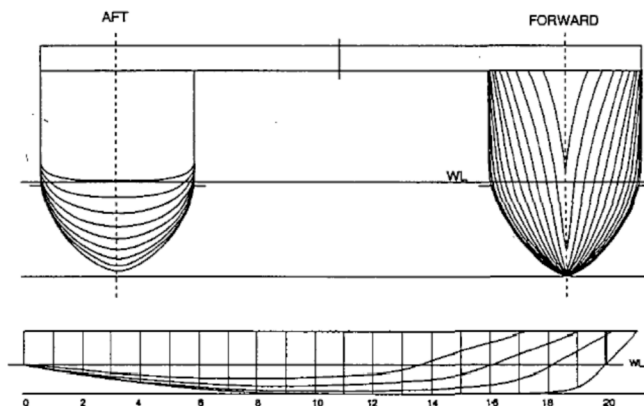


Fig. 1. Basic geometry definition and body plan of the Delft 372 catamaran model.



Fig. 2. CNR-INSEAN-2554 model for towing-tank seakeeping experiments at INSEAN.

Table 1
Main particulars of the CNR-INM model 2554.

Particular	Symbol	Unit	Value	
			Model	Full
Scale	Λ	-	33.33	-
Length between perpendiculars	L_{pp}	m	3.00	100.00
Beam overall	B	m	0.94	31.33
Beam demi-hull	b	m	0.24	8.00
Distance between center of the demi-hulls	H	m	0.70	23.33
Draught	T	m	0.15	5.00
Displacement	Δ	kg	87.0	3225000
Vertical center of gravity	KG	m	0.34	11.33
Longitudinal center of gravity	LG	m	1.41	47.00
Pitch radius of gyration	K_{yy}	m	0.782	26.07

deck-slaming phenomena occurred during the tests. The total weight and its distribution are carefully checked in order to match the prescribed displacement and dynamical properties.

Current regular and irregular wave tests are focused on first and second harmonic components of the dynamical (resistance) and kinematic (motions) quantities. Therefore, the experimental setup should be able to provide time accurate measurements of loads and motions. Different linking systems have been tested. The first one was not completely rigid, so that (as it will be shown later) the motion of the beam induced a large elastic response of the mounting system, leading to a large over prediction of both added resistance and the amplitude of its second harmonic component. This problem was particularly evident due to the high speed at which the catamaran has been tested. To overcome this issue, a second more rigid mounting solution was designed and built (as in Fig. 3). This new arrangement was tested either with or without soft springs. As it will be shown later, the use of soft springs works as a low pass filter, damping out first and higher harmonics, thus providing the mean in wave resistance only. On the contrary, without springs, the system has been tested and verified to provide accurate measurements without any large deformation which would affect the measurements themselves.

2.2. Instrumentations

2.2.1. Motion measurements

A Krypton optical system with an acquisition frequency of 800 Hz, is used to measure the motion of the model. It consists of three linear CCD cameras (K600 camera unit) which detect the position of a reference system fixed to the body (identified through three infrared LEDs); the plate with the infrared LEDs is placed in the stern region of the left hull, as sketched in Fig. 4.

The spatial position of each LED is found with a high resolution through a triangulation procedure. The field of view of the cameras spans from 1.5m to 6m; the accuracy of the system is distributed in three

Particular	Symbol	Unit	Value	
			Model	Full
Scale	Λ	-	33.33	-
Length between perpendiculars	L_{pp}	m	3.00	100.00
Beam overall	B	m	0.94	31.33
Beam demi-hull	b	m	0.24	8.00
Distance between center of the demi-hulls	H	m	0.70	23.33
Draught	T	m	0.15	5.00
Displacement	Δ	kg	87.0	3225000
Vertical center of gravity	KG	m	0.34	11.33
Longitudinal center of gravity	LG	m	1.41	47.00
Pitch radius of gyration	K_{yy}	m	0.782	26.07

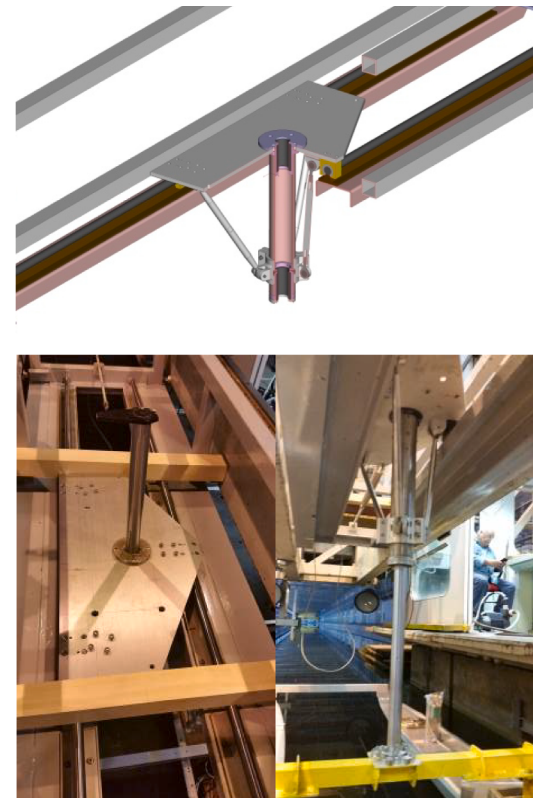


Fig. 3. Details of the mount system.



Fig. 4. Sketch of the plate with infrared LEDs placed on the hull.

zones:

- Zone I: From 1.5m to 3.5m with a vol. accuracy of $0.09 + 0.01$ mm/m and a single point accuracy of $0.060 + 0.007$ mm/m
- Zone II: From 3.5m to 5.0m with a vol. accuracy of $0.09 + 0.025$ mm/m and a single point accuracy of $0.060 + 0.017$ mm/m
- Zone III: From 5.0m to 6.0 m with a vol. accuracy of $0.190 + 0.025$ mm/m and a single point accuracy of $0.130 + 0.017$ mm/m

where the measurement uncertainty is expressed for a confidence level of 95%, according to ISO 10360 II standard. In the current setup, the distance between the CCD cameras and the target plate is 2.5m, therefore the Zone I is the reference one with a global accuracy of $0.225 + 0.025$ mm and a single point accuracy of $0.150 + 0.017$ mm.

2.2.2. Resistance measurements

For the direct measurement of the total resistance in waves, two OMEGA LC204 load cells with maximum range of 445N and accuracy around 0.1% are used. They are designed to be surface mounted with the load applied through the mounting stud. The cells are placed between the gimbal and the ship model, one for each gimbal. The added resistance in the ship frame of reference (*i.e.* along the longitudinal axis of the catamaran) results from the subtraction of the calm water resistance to the average value of the total resistance in waves. Since the load cells are mounted on the hull, non-inertial effects should be estimated and subtracted. To this aim, the required time histories of the acceleration in correspondence of the cells positions have been reconstructed from the measurements of the motion.

2.2.3. Acceleration measurements

The acceleration of the model is measured at the Bridge and at the Flight Deck; two accelerometers are placed at the following positions:

- Bridge Accelerometer: Horizontal $0.30L_{PP}$ from the Front Perpendicular (FP), Vertical $0.15L_{PP}$ from the keel line or dimensionally 90 cm from FP and 45 cm from the keel line.
- Flight Deck Accelerometer: Horizontal $0.85L_{PP}$ from the FP, Vertical $0.10L_{PP}$ from the keel line or dimensionally 255 cm from FP and 30 cm from the keel line (the accelerometer is visible in Fig. 4).

The flight deck velocity is obtained through time integration.

2.2.4. Incoming wave measurements

The elevations of the incident waves are measured at two different stations. The first one at 3m ahead the model, which is considered as the measurement of the undisturbed incident wave, while the second measurement is acquired by a probe placed approximately 3m aside the hull at the LCG position (see Fig. 5); this wave measurement could be partially affected by the hull (for lower speeds), but it is only used to compute the phase shift between the incident wave and the motion of the catamaran. The wave height has been measured by means of Kenek probes, which is a non-intrusive instrumentation with accuracy of 0.1 mm and a maximum range of measurement of 150 mm. This probe is suitable for low speed seakeeping tests and moderate wave steepness, therefore it has been considered accurate enough for the wave steepness range and Fr number at which the present tests are carried on.

2.3. Facility, wave maker validation

Sea keeping tests are performed in the “Emilio Castagneto” towing tank, one of the CNR-INM (formerly CNR-INSEAN) facilities, which dimensions are: 220m, 9m and 3.6m in length, width and depth, respectively. The tank is equipped with a towing carriage capable to operate at the maximum speed of 15.0 m/s; carriage speed fluctuations are less than 0.01%. Head wave system is generated by means of a Kempf & Remmers wave maker. The wave maker is equipped with a flap plunger hinged 1.80m below the calm water level, with a maximum angle range $\pm 13^\circ$, frequency range 0.1–1.8 Hz. In order to ensure reliable and accurate seakeeping test measurements, the wave maker has been recently revamped and its performances (*i.e.* accuracy and repeatability of the generated wave systems) have been carefully evaluated. A campaign for the qualification of the facility has been performed; it involved the estimation of the transfer function of the plunger stroke versus the frequency, the determination of the frequency response function of the mechanical system and the estimation of the error and repeatability of the generated waves. The validation assessment has been performed for the whole operating range of the system. The generated wave system has been measured by probes mounted on several transversal beams placed all along the channel length, allowing the estimation of both the two-dimensionality of the wave, its dissipation along the tank and possible reflections from the basin end (which should be dampened by the presence of the absorbing beach).

Validation assessments for the regular wave generation are reported in Table 2; three height over wave length ratios in the whole range of the operating frequencies of the wave maker have been tested. The test covers the generation of the regular waves from linear ($kA = 0.052$) to high non-linear ($kA = 0.209$) ranges. As clear from Table 2, low errors (up to 5%) are estimated for linear and weakly non-linear ($kA < 0.1$) waves whereas, as expected, higher errors (and unsatisfactory repeatability) are observed for highly non-linear waves ($kA > 0.1$). Moreover, larger errors and uncertainties are generally seen for higher frequencies, regardless the wave steepness ($f > 1$ Hz, *i.e.* shortest waves); this indicates that the flap plunger of the wave maker (activated by a hydraulic servomechanism) experiences difficulties to generate high frequency waves. Moreover, negligible reflection from the basin ends and poorly significant wave damping along the basin have been observed. However, it has to be noticed that the regular wave tests that will follow are pursued for a frequency/steepness range for which the error (in the amplitude) is not larger than 5%, whereas, this limit is partially overtaken in the irregular wave tests. Error and uncertainty in the generation of an irregular wave system has been verified only for the condition under analysis in this paper and it will be presented in section 4.1.2.

3. Statistical variables and methodss

The methodology for stochastic uncertainty quantification employed

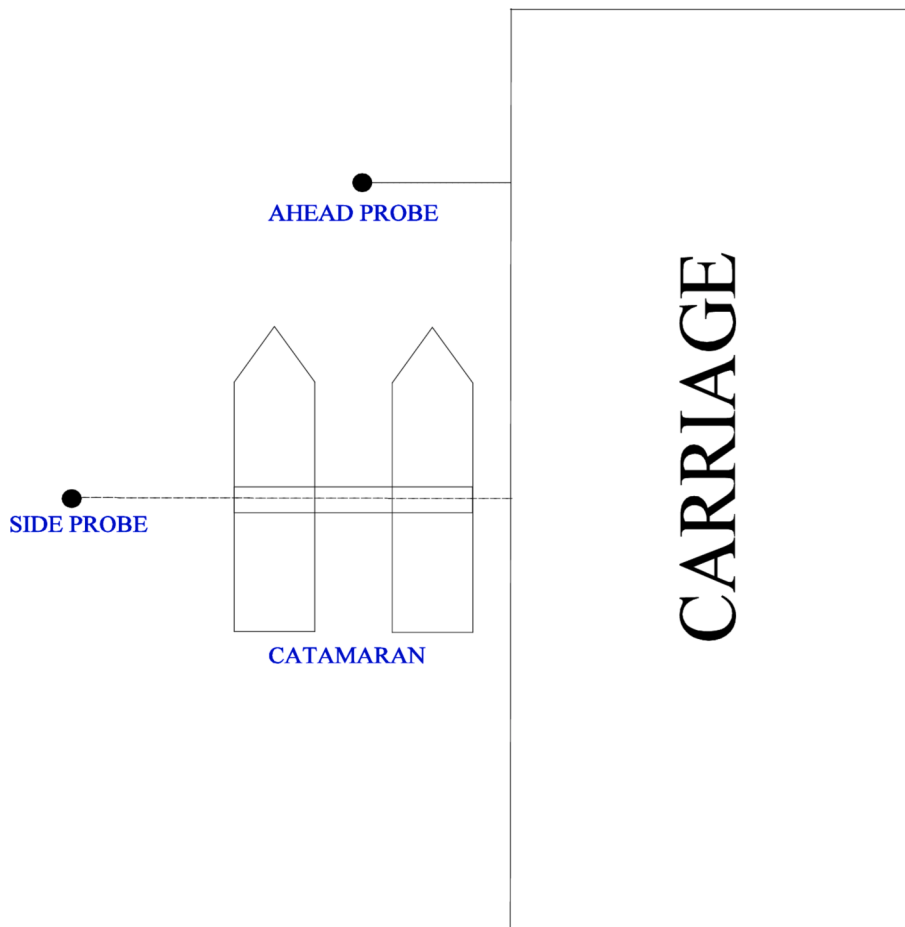


Fig. 5. Scheme of probes positions.

Table 2

Wave maker calibration, estimation of the error and uncertainty of the generated regular wave.

kA	H/λ	f[Hz]	λ [m]	H[cm]	σ[%H]	E[%H]
0.052	1/60	0.1	57.98	96.63		2.03%
		0.3	15.55	25.92		2.66%
		0.5	6.24	10.40	1.25%	2.77%
		0.7	3.19	5.32		3.10%
		0.8	2.44	4.07		4.20%
		0.9	1.93	3.22	1.58%	4.62%
		1.1	1.29	2.15		5.30%
		1.3	0.92	1.53	>15%	>10%
		1.5	0.69	1.15		>10%
		1.8	0.48	0.80		>10%
0.105	1/30	0.5	6.24	20.80	0.60%	2.80%
		0.9	1.93	6.43	3.74%	2.85%
		1.3	0.92	3.07	>15%	>10%
0.209	1/15	0.5	6.24	41.60	>10%	>10%
		0.9	1.93	12.87	>10%	>10%
		1.3	0.92	6.13	>10%	>10%

in this work follows the one already used in Diez et al. (2018b); however, for the sake of completeness the methodology is also briefly recall here. The validation variables are the wave elevation ζ , x-force (positive forward), heave z_G (positive upward), pitch angle θ (positive bow up), vertical acceleration of the bridge \dot{z}_B (positive upward), and vertical velocity of the flight deck \ddot{z}_D (positive upward). Time series values are addressed as primary variables, whereas mean-crossing amplitudes, height and period are indicated as secondary variables. The subsamples and bootstrap methods are applied in order to estimate the validation values and 95% confidence intervals for expected value (EV), standard

deviation (SD) and quantile function. Additionally, validation values and confidence intervals for time series EV and SD are evaluated by time series theory, based on the sample variance and size, and the autocovariance function. The stochastic regular wave UQ focuses on SSA's of pitch, acceleration and velocity as relevant merit factors for design optimization.

3.1. Statistical estimators and confidence intervals for irregular wave benchmark

3.1.1. Statistical variables

Statistical variables of interest are expected value (EV), standard deviation (SD), and cumulative distribution function (CDF), probability density function (PDF), or quantiles, along with the mode. They are evaluated numerically for both primary and secondary variables using a sample of N items. For primary variables, items are extracted from the time series as $J_i = J(t_i)$, $i = 1, \dots, N$. For secondary variables, N mean-crossing waves are identified and the associated J_i defined. Note that the sample size N is different for primary and secondary variables.

The statistical estimators are evaluated as follows:

$$EV(J) = \frac{1}{N} \sum_{i=1}^N J_i \quad (1)$$

$$SD(J) = \sqrt{\frac{1}{N-1} \sum_{i=1}^N [J_i - EV(J)]^2} \quad (2)$$

$$CDF(J, y) = \frac{1}{N} \sum_{i=1}^N \delta[J_i \leq y] \quad (3)$$

The PDF is evaluated using here the kernel density estimate (Silverman, 1986) as

$$PDF(J, y) = \frac{1}{Nh} \sum_{i=1}^N K\left[\frac{y - J_i}{h}\right] \quad (4)$$

where K is a normal kernel function

$$K[x] = \frac{1}{\sqrt{2\pi}} \exp\left(-\frac{x^2}{2}\right) \quad (5)$$

and h is a bandwidth defined here by the following rule of the thumb (Silverman, 1986)

$$h = SD(J) N^{-\frac{1}{5}} \quad (6)$$

3.1.2. Statistical estimators and confidence intervals of primary variables

3.1.2.1. Autocovariance matrix method (AC). The analysis of the autocovariance matrix is used to provide validation values and confidence intervals for EV and SD of time series values (primary variables). The formers are provided directly by Eqs. (1) and (2). Following the work by Belenky et al. (2015) (Belenky et al., 2013) the confidence intervals associated to a single wave record are evaluated using the variance of the mean $Var(EV)$ and the variance of the variance $Var(SD^2)$. The former is

$$Var(EV) = Var_S(EV) + Var_R(EV) \quad (7)$$

where

$$Var_S(EV) = \frac{SD^2}{N} \quad (8)$$

is the contribution to the variance of the mean associated to the diagonal terms of the autocovariance matrix and

$$Var_R(EV) = \frac{2}{N} \sum_{i=1}^{N-1} \left(1 - \frac{i}{N}\right) R(\tau_i) \quad (9)$$

is the contribution to the variance of the mean associated to the off-diagonal terms, stemming from the dependence of the time series items, evaluated through the autocovariance function as

$$R(\tau_i) = \frac{1}{N-i} \sum_{j=1}^{N-i} [J_j - EV(J)] [J_{j+i} - EV(J)] \quad (10)$$

Here, a weighted autocovariance function (Belenky et al., 2015) of the form

$$\hat{R}(\tau_i) = \frac{1}{N} \sum_{j=1}^{N-i} [J_j - EV(J)] [J_{j+i} - EV(J)] \quad (11)$$

is used.

The statistical uncertainty associated to EV is evaluated at the 95% confidence level assuming a normal distribution for the EV estimate as

$$U_{EV} = 2\sqrt{Var_S(EV) + Var_R(EV)} = 2\sqrt{Var(EV)} \quad (12)$$

Similarly to $Var(EV)$, the variance of the time series variance $Var(SD^2)$, is

$$Var(SD^2) = Var_S(SD^2) + Var_R(SD^2) \quad (13)$$

where, assuming normally distributed items,

$$Var_S(SD^2) = \frac{2SD^4}{N} \quad (14)$$

and

$$Var_R(SD^2) = \frac{4}{N} \sum_{i=1}^{N-1} \left(1 - \frac{i}{N}\right) [R(\tau_i)]^2 \quad (15)$$

The statistical uncertainty associated to SD is evaluated at the 95% confidence level by the central-limit theorem as (Belenky et al., 2013)

$$\frac{U_{SD}}{SD} = \sqrt{1 + 2 \frac{\sqrt{Var_S(SD^2) + Var_R(SD^2)}}{SD^2}} - 1 \quad (16)$$

3.1.2.2. Non-overlapping block-bootstrap method (NBB). In order to define the validation values and confidence intervals of the statistical estimators of Eqs. (1)–(4), a NBB method (Broglio et al., 2019) (Künsch, 1989) (Politis and Romano, 1994; Politis et al., 1999) is applied to the time series, using a number of $C = \lfloor N/l \rfloor$ non-overlapping blocks, where l is an optimal block length given by

$$l = (2\phi/c)^{2/3} N^{1/3} \quad (17)$$

with

$$\phi = \frac{N \sum_{i=1}^{N-1} [J(t_{i+1}) - EV(J)][J(t_i) - EV(J)]}{(N-1) \sum_{i=1}^N [J(t_i) - EV(J)]^2} \quad (18)$$

and $c = (1 - \phi)(1 + \phi)$.

From the original C blocks, a number of C blocks are drawn at random with replacement and concatenated in the order they are picked, forming a new (bootstrapped) series of size N . A number of $B = 100$ bootstrapped series is used in the current analysis.

EV and SD are evaluated as per Eqs. (1) and (2). The CDF is assessed by the quantile function q , evaluated at probabilities $p = 0.025, 0.1, 0.2, \dots, 0.8, 0.9, 0.975$. If one sorts all the $J(t_i)$, $i = 1, \dots, N$ within each bootstrapped series, such that $J(t_{i-1}) \leq J(t_i) \leq J(t_{i+1})$, then

$$q(p) = J_{[pN]} \quad (19)$$

The validation value for EV and its 95% confidence lower and upper bounds are evaluated respectively as

$$EV = \text{Median}(EV_b) = EV_{[0.5B]} \quad (20)$$

$$EV_l = EV_{[0.025B]} \quad (21)$$

$$EV_u = EV_{[0.975B]} \quad (22)$$

where EV_b represents the EV value of the b -th bootstrapped series, ordered such as $EV_{b-1} \leq EV_b \leq EV_{b+1}$. Finally,

$$U_{EV} = 0.5(EV_u - EV_l) \quad (23)$$

The validation values and the confidence intervals for SD and q are evaluated similarly to EV, as per Eqs. (20)–(22).

3.1.2.3. Moving block-bootstrap method (MBB). In addition, and for comparison to the NBB method, validation values and confidence intervals of the statistical estimators of Eqs. (1)–(4) are evaluated using a MBB method (Broglio et al., 2019), (Künsch, 1989; Miecznikowski et al., 2010b; NATO STANAG 4154, 1997; Politis and Romano, 1994; Politis et al., 1999). In the case of moving blocks, the original blocks (to pick from) are in number $C = N - l + 1$, each formed by $J(t_i)$, $i = j, \dots, j + l - 1$, where j is the block index and l is evaluated as in the NBB method. From the original set of C blocks, a number of $C' = \lfloor N/l \rfloor$ blocks are drawn at random with replacement and concatenated in the order they are

picked, forming a new (bootstrapped) series of size N . A number of $B = 100$ bootstrapped series is used in the current analysis. The validation value for EV, SD, mode, and q with their 95% confidence lower and upper bounds are evaluated as in the non-overlapping block bootstrap method.

3.1.3. Statistical estimators and confidence intervals of secondary variables by the bootstrap method

The validation values and confidence intervals of the secondary variables are calculated using the bootstrap method (Efron, 1981). The method consists in constructing an empirical probability distribution from the sample (assumed independent and identically distributed) by assigning a probability of $1/M$ to each item. This empirical probability distribution function represents the nonparametric maximum likelihood estimate of the (unknown) actual distribution. The associated empirical CDF is given by Eq. (3). From the empirical CDF, calculate a number of B new sets (bootstraps), each of which contains new random items J_i^* , $i = 1, \dots, M$ defined as

$$J_i^* = CDF^{-1}(p_i) \quad (24)$$

where p_i are M uniformly distributed random items in $[0; 1]$. In practice, if one orders the original items J_i such as $J_{i-1} \leq J_i \leq J_{i+1}$, the new items J_i^* are

$$J_i^* = J_{[p_i M]} \quad (25)$$

Validation values and 95% confidence intervals for EV, SD, mode and quantiles are evaluated similarly to block bootstrap methods, where b indicates values from the b -th bootstrap.

3.2. Statistical estimators and confidence intervals of regular wave UQ model

Regular wave UQ models have been developed for variables relevant to design optimization (Diez et al., 2013, 2014, 2018a). Specifically, bi and uni-variate UQ models have been applied to ship response predictions considering the wave period, height and frequency as stochastic variables (Diez et al., 2018a). The uni-variate UQ model considering stochastic wave frequency is used here for the EV of the X-force and the SD of the motions whose maximum Single Significant Amplitude (SSA) is prescribed by the NATO STANAG 4154 standardization agreement (NATO STANAG 4154, 1997). A Latin-hypercube Monte Carlo method with importance sampling is applied, using a number of L uniformly-distributed regular wave experiments from metamodel predictions by radial basis functions (Volpi et al., 2015).

The EV for the force is then evaluated as:

$$\begin{aligned} -EV(F_x) - R_{CW} &= EV\left(2m_0 \frac{-EV_i(F_x) - R_{CW}}{A_i^2}\right) = \\ &\left[\sum_{i=1}^L f(\omega_i)\right]^{-1} \sum_{i=1}^L 2m_0 \frac{-EV_i(F_x) - R_{CW}}{A_i^2} f(\omega_i) \end{aligned} \quad (26)$$

where R_{CW} is the calm water resistance and the subscript i indicates the i -th regular wave experiment at wave height equal (in the present work) to the average height of the Rayleigh distribution,

$$2A_i = \bar{H} = \sqrt{\frac{\pi}{8}} H_s \quad \text{for all } i \quad (27)$$

and period $T_i = 2\pi/\omega_i$. A_i is the amplitude of the i -th regular wave. The probability density function is defined as $f(\omega_i) = S(\omega_i)/m_0$, where m_0 is the spectrum energy (zero-th moment).

The SD^2 of θ , a_B , and z_D is computed as

$$[SD(J)]^2 = EV[\hat{\sigma}_i^2(J)] = \left[\sum_{i=1}^L f(\omega_i)\right]^{-1} \sum_{i=1}^L \hat{\sigma}_i^2(J) f(\omega_i) \quad (28)$$

where, using the moment transport theorem,

$$\hat{\sigma}_i^2(J) = 2m_0 \frac{\left[EV_i(J) - \frac{1}{L} \sum_{i=1}^L EV_i(J)\right]^2}{A_i^2} \quad (29)$$

Herein, the metamodel presented in (Volpi et al., 2015) is used to predict EV_i and SD_i in Eq. (29), versus the wave frequency. The confidence intervals for EV_i and SD_i are approximated here by Eqs. (12) and (16), without considering the non-diagonal terms in the autocovariance matrix. Finally, $SSA = 2 SD$.

4. Seakeeping tests

The North Pacific Ocean environment has been selected as the operating conditions in a real scenario; this choice was motivated by the wide literature on the energy spectral distributions obtained from measurement campaigns by off-shore industries. In Table 3 the characteristics of the North Pacific Ocean are indicated: the mean wave height (trough to crest) of the highest third of the waves ($H_{1/3}$) and the most probable modal wave period (T_m) are shown for sea states from 1 to 8.

Following Diez et al. (2013), a 100m full-scale length catamaran (advancing in head waves) is considered with a variable operational speed within the range from $Fr = 0.115$ to 0.575 ; in the present work an average Froude number of 0.425 and a sea state 5, highlighted in Table 3, are chosen. The operational environment is then characterized by a significant wave height $H_{1/3}$ of 3.25 m at full scale (corresponding to 95.5 mm at model scale). This yields the mean wave height $H_m = \sqrt{\frac{2}{3}} H_{1/3}$ to 2.04 m at full scale, which corresponds to 61.10 mm at model scale. The most probably wave period T_m corresponds to the modal frequency of 9.7 s at full scale and 1.68 s at model scale.

In Table 4 the main sea characteristics are indicated: it is worth to notice that the maximum steepness is close to the linearity limit.

4.1. Irregular wave tests

The irregular wave system has been generated by considering the Bretschneider energy spectrum, which is the best representation of the present scenario, being developed for modeling the North Pacific area. From the linear theory it is known (see Falinsen (2005)) that the total energy of a single monochromatic wave of amplitude η is $\rho g \eta^2/2$. In the case of irregular sea, a spectral analysis of the gravity wave amplitudes leads to a similar definition for the energy amount associated to a wave with a specific frequency ω

$$\frac{1}{2} \rho g \eta^2(\omega) = E(\omega) \Delta\omega \quad (30)$$

and, from the definition of the energy density $S(\omega) = E(\omega)/(\rho g)$, it simply reduces to

$$\frac{\eta^2(\omega)}{2} = S(\omega) \Delta\omega \quad (31)$$

Obviously, the wave amplitude spectrum depends on the interval $\Delta\omega$ chosen, because the energy carried by a single wave component depends on the integral of $S(\omega)$ over the considered frequency interval.

The spectrum $S(\omega)$ is usually expressed in the form:

$$S(\omega) = \frac{A}{\omega^5} \exp\left(-\frac{B}{\omega^4}\right) \quad (32)$$

where the definition of A and B is arbitrary and normally is referred to the desired sea environment. For the Bretschneider spectrum:

Table 3

Characteristic annual values for sea states in North Pacific.

Sea State	Mean $H_{1/3}$ [m]	Probability of sea state (%)				Most probable modal wave period T_m [s]		
		Bales, 1982	Lee and Bales, 1984	Average	Exceedance	Bales, 1982	Lee and Bales, 1984	Ave.
0–1	0.05	0.00	1.30	0.65	99.35	–	–	–
2	0.30	4.10	6.40	5.25	94.10	7.50	6.30	6.9
3	0.88	16.90	15.50	16.20	77.90	7.50	7.50	7.5
4	1.88	27.80	31.60	29.70	48.20	8.80	8.80	8.8
5	3.25	23.50	20.94	22.22	25.98	9.70	9.70	9.7
6	5.00	16.30	15.03	15.67	10.32	13.80	12.40	13.1
7	7.50	9.10	7.60	8.35	1.96	13.80	15.00	14.4
8	11.50	2.20	1.56	1.88	0.08	18.00	16.40	17.2
>8	>14	0.10	0.07	0.09	0.00	20.00	20.00	20

Table 4

Irregular wave parameters.

Quantity	Symbol	Full	Model
Speed of Advancement	U [m/s]	13.3091	2.305
	U [kn]	25.8711	4.481
Froude Number	$Fr-J$	0.425	
Mean value of 1/3 largest wave	$H_{1/3}$ [m]	3.2500	0.0975
Mean wave height	H_m [m]	2.0366	0.0611
RMS of wave height	H_{rms} [m]	2.2981	0.0689
Encountering frequency (minimum)	f_e [Hz] min	0.0800	0.4619
Encountering frequency (maximum)	f_e [Hz] max	0.4000	2.3094
Wave frequency (minimum)	f [Hz] min	0.0546	0.3077
Wave frequency (maximum)	f [Hz] max	0.1657	0.9569
Wave length (minimum)	λ [m] min	56.8146	1.7045
Wave length (maximum)	λ [m] max	523.7561	14.9574
Non dimensional wave length (minimum)	λ/L_{pp} min	0.5681	0.5682
Non dimensional wave length (maximum)	λ/L_{pp} max	5.2376	4.9858
Minimum H_m over wave length	H_m/λ min	0.0039	0.0041
Maximum H_m over wave length	H_m/λ max	0.0358	0.0358
Steepness (minimum)	kA min	0.0122	0.0128
Steepness (maximum)	kA max	0.1126	0.1126

$$S(\omega) = \frac{5}{16} \frac{\omega_m^4}{\omega^5} H_{1/3}^2 \exp\left(-\frac{5}{4} \frac{\omega_m^4}{\omega^4}\right) \quad (33)$$

where ω_m is the peak (modal) angular frequency and $H_{1/3}$ is the significant wave height, whereas $T_m = 2\pi/\omega_m$ is the period associated to the modal frequency. The system of irregular waves is then generated by a linear superposition of elemental wave components:

$$\eta(t) = \sum_{k=1}^{N_w} A_k \cos(\omega_k t + \varphi_k) \quad (34)$$

where N_w is the number of components, $A_k = \sqrt{2S(\omega_k)\Delta\omega}$ and φ_k is a random phase. For both the validation test and the irregular seakeeping tests of the catamaran, the wave is generated using $N_w = 993$ components, ranging from 0.18 to 1.84 Hz (wider than the range of the regular wave frequencies reported in Table 4).

4.1.1. Irregular wave generation: validation

Before proceeding to seakeeping tests, the wave maker has been validated in order to assess its capabilities in reproducing the required sea state. To this end, ten acquisitions of the wave amplitudes have been performed; acquisitions are made in a fixed point of the basin, about 25m from the wave maker. Each recording lasts 250s.

The time history of the wave height (including its running mean and RMS) for one acquisition is depicted in Fig. 6: it is worth to underline that a satisfactory convergence for both the mean and the RMS of the wave height has been achieved after each run. The ten acquisitions have been post-processed in order to evaluate the global spectrum, as well as the spectra of each single acquisition to inspect their convergence toward the theoretical one. This approach allows assessing the minimum recording time required for the seakeeping test: when the catamaran has

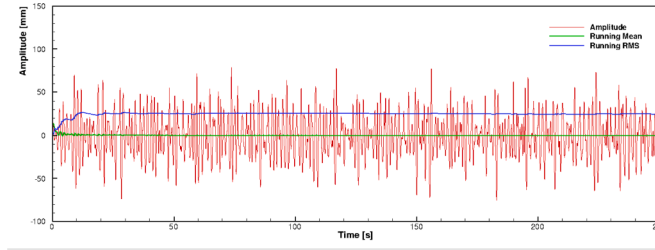


Fig. 6. Wave Amplitudes, running means and RMS for one validation acquisition.

encountered a well enough reproduced sea spectrum, the acquisition time may be considered good for the estimation of the statistics.

In Fig. 7 the energy densities spectra obtained by the wave amplitude time signal are shown. The smooth curves are obtained through a natural smoothing spline approximation of the original data with a reconstruction via piecewise cubic polynomials with 1000 segments for each curve. The endpoints of each segment are interpolated. The figure depicts the spectrum convergence, obtained by doubling the number of samples; a clear distinction among the different distributions is evident near the peak and at higher frequencies. In particular, it should be noticed that the convergence is monotonic in the range 0.2Hz–0.5 Hz where the wave behavior is fundamentally linear. On the contrary, at high frequencies (>0.9 Hz) no convergence toward the theoretical spectrum is detectable. In the medium range 0.5Hz–0.9 Hz a convergence in the peak values, highlighted in the side table of Fig. 7, is evident although oscillating (but monotonic in magnitude). The results are very encouraging for low frequencies (i.e. frequencies lower than 0.5 Hz), where the wave maker is highly reliable. Conversely, for higher frequencies (higher than 0.8 Hz) the spectra manifest an evident energy increase with respect to the theoretical one; this effect is mainly ascribable to the difficulty of the wave maker in accurately producing short wavelengths, standing the mechanical limits of the flap plunger. Quantitative error estimation is not trivial: an L^2 norm of the relative error with the theoretical spectrum within the whole frequencies range could be meaningless, because of the flap plunger problems at high frequencies explained above. Moreover, when an experimental campaign of measurement is carried out, the error on the total energy content and on the position and intensity of the energy density peak are, by far, more important than the local error on $S(\omega)$. For this reason, a convergence based on the peak error and on the global energy is preferred. The global error is calculated as the difference between the theoretical and the measured integrals of the energy densities evaluated between ω_{min} and ω_{max} . These latter are, respectively, the lower and higher frequency corresponding to an energy density the 5% of the theoretical spectrum peak (in this case $\omega_{min} \sim 0.4$ Hz, $\omega_{max} \sim 1.38$ Hz), as suggested by the ITTC guidelines (Load and Responses Commit, 2002). The percentage error between the energy peak of the measured spectrum and the theoretical one is shown in the second column of the side

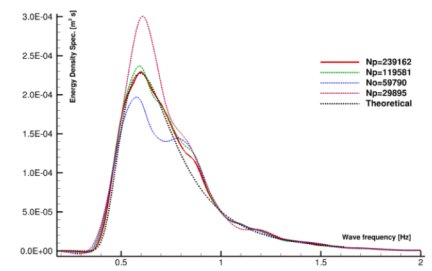


Fig. 7. Energy spectrum convergence by doubling the number of samples respect to the wave frequency. In the table the peak and the global integral error of the spectra respect to the theoretical one.

table of Fig. 7 while the total energy is reported in the third column. As anticipated, the convergence in terms of the peak intensity is quite monotonic (in magnitude), whereas an oscillating behavior is observed in terms of total energy; nevertheless, a satisfactory error is seen, with values lower than 6% for the latter and lower than 1% for the peak error.

Once the spectrum can be assumed to correctly represent the theoretical one, the calculation of the second and fourth momenta are useful to verify that the bandwidth coefficient, suggested by Mollison (Mollison and EvansFalcão, 1985), falls in the correct range:

$$\varepsilon = \sqrt{1 - \frac{m_2^2}{m_0 m_4}} \cong 0.59 \quad (35)$$

which is in satisfactory agreement with the theoretical value of 0.56. It should be pointed out that, for an ocean environment, a typical broadband value of $0.5 < \varepsilon < 0.6$ is expected, so that the present value means that the sea spectrum produced is really representing an ocean environment.

The measured statistics of the generated sea are reported in Table 5. As expected, the value of $H_{1/3}$ obtained from the measurements (101.76 mm) is close to the expected value of 97.5 mm indicated in Table 3, with a percentage error of 4.37%. The total number of encountered waves (N_w) is a quite vague value that can be calculated in different manners. From a direct evaluation of the negative zero-crossing it would be equal to 1825 but, by considering the mean zero crossing period $\bar{T}_{zc} = \sqrt{m_2/m_0} \sim 1.27s$, this value rises to 1879. However, if the average peak-to-peak period $\bar{T}_c = \sqrt{m_4/m_2} \sim 1.02s$ is taken into account, the final number of encountered waves becomes 2337. By stressing the information coming from the spectrum and being the data in agreement with a raw measurement of zero crossing events, the value of 1879 will be considered hereafter.

In the left frame of Fig. 8 the running means and RMS are highlighted for the global time history, showing the asymptotic value of ~ 25.98 mm which represents the standard deviation. In the right plot of Fig. 8, the amplitude percentage occurrence of the irregular waves shows a correct Gaussian distribution.

Finally, in order to exclude unwanted periodic signals in the stochastic realizations of the experiments, the autocorrelation function is evaluated. The autocorrelation is the correlation of a signal with a delayed copy of itself as a function of delay τ . Differently from the PDF, which contains information on the amplitude variation of the process, the autocorrelation gives an indication of the time variation of the process, allowing to evaluate periodic patterns even if they are covered by a white noise. It is defined by the formula:

Table 5

Wave statistics on the sea state generated with a Bretschneider spectrum (wave heights and RMS are in millimetres at model scale).

RMS	$A_{1/3}^+$	$A_{1/3}$	$H_{1/3}$	A_{MAX}^+	A_{MAX}	H_{MAX}	N_w
25.98	56.53	-49.60	101.76	99.99	-90.67	186.27	1879

Samples	Peak E %	Global E %
29895	31.97%	19.8%
59790	13.39%	2.50%
119581	4.13%	8.25%
239162	0.77%	5.87%

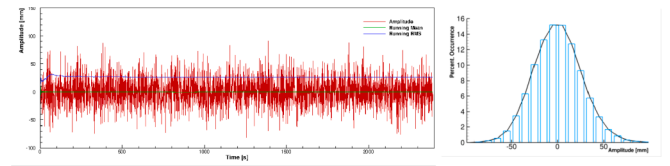


Fig. 8. Left: Time histories of waves amplitudes, running means and RMS for the irregular waves experiment. Right: Percentage occurrence of the Wave Amplitudes.

$$R\left(\tau_i\right) = \frac{1}{SD^2} \sum_{k=1}^{N-i} E\{[(J(t_k) - EV(J))(J(t_{k+i}) - EV(J))\} \quad (36)$$

where τ_i is the time lag and $E(X)$ is the expected value operator. If a signal varies slowly in time, its value at times t and $t + \tau$ remains quite similar and the autocorrelation will be positive, while, if it varies quickly, the autocorrelation will assume a value close to zero. In Fig. 9 the autocorrelation for the time signals of all the measured quantities is reported, demonstrating that any periodic pattern is present in the time signals and they are only related to stochastic processes.

4.1.2. Irregular wave tests

Once the capabilities of the wave maker in correctly reproducing the required sea state have been appraised, the seakeeping tests have been performed. The experiments were carried out at the reference speed of 2.305 m/s (model scale), i.e. at a length based Froude number equal to 0.425. By taking into account an operative length of 220m for the towing tank, the time window for each run is approximately 95s. Excluding the transient phases (acceleration and stop), a useful time window of about 50s may be assumed for each run. This means that in each test about 289s at full scale are simulated. According to the ITTC recommended procedures and guidelines (Load and Responses Commit, 2002), the test duration should cover at least 30 min of equivalent full scale. This means that measurement must be recorded for, at least, 6 runs; in the present analysis, for an accurate evaluation of the statistics and in order to guarantee good convergence properties, 18 runs were considered. The total time of acquisition corresponds to 86.6 min at full scale, exceeding almost 3 times the ITTC recommendations.

As already stated, the considered sea spectrum is the Bretschneider one, with characteristics defined in the previous section. The final data are obtained by concatenating the 18 runs through fading in/out ramps with a length of about 1.5 modal periods, such ensuring negligible frequency analysis errors. According to the current setup, the number of time samples is $N = 90114$, this assures the model to encounter 1464 waves (see Table 6).

In addition to the validation reported in the previous subsection, the quality of the irregular wave system has been further validated; its accuracy is summarized in Table 6, where zero, first and second order spectrum moments are compared with the theoretical values; the errors

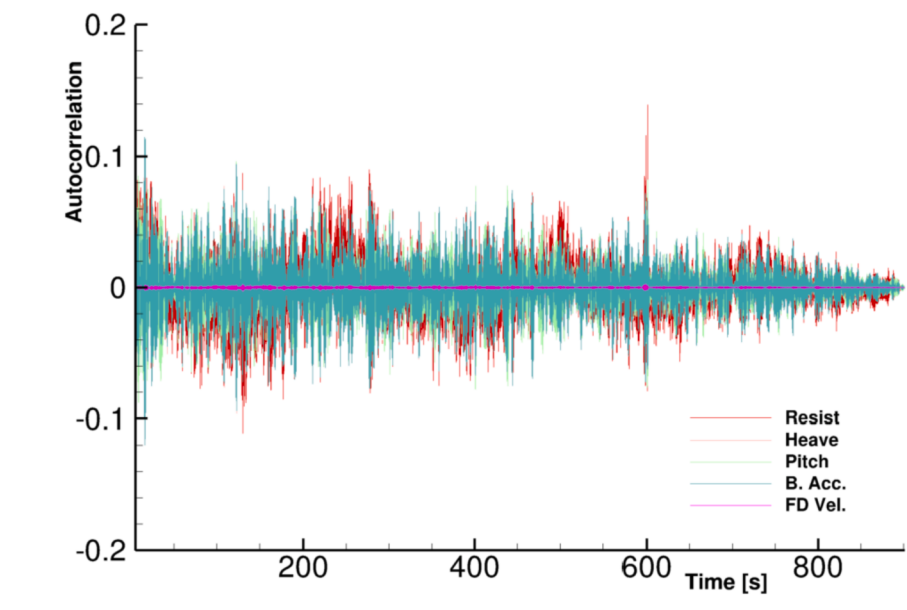


Fig. 9. Autocorrelation function for all the measured quantities.

Table 6

Irregular wave statistical analysis and uncertainty estimate through energy spectrum – wave elevation.

N. runs	Total enc. waves	m_0		m_1		m_2		Ave. $ E \%$
		Value [m^2]	$ E \%$	Value [$m^2 \text{ Hz}$]	$ E \%$	Value [$m^2 \text{ Hz}^2$]	$ E \%$	
18	1464	$8.71 \cdot 10^{-5}$	1.41%	$6.13 \cdot 10^{-5}$	0.17%	$4.65 \cdot 10^{-5}$	0.02%	0.53%

are generally less than 1.5%, decreasing for the higher moments, with an average error of about 0.5%.

Table 7 shows the UQ assessment of the encountered wave train. The validation study includes the wave elevation as primary variable and the wave height as secondary variable. The wave elevation and its autocovariance are presented in Fig. 10.

The wave elevation statistics is assessed by autocovariance analysis and both non-overlapping and moving block bootstrap methods (see Table 7). Errors of EV, SD and quantiles versus theoretical values are reasonable, being smaller than 3%. The associated uncertainties are also rather small (less than 3%). The wave height statistics have a similar trend with larger errors and uncertainties.

Fig. 11 shows the PDFs and the quantiles of wave amplitude and the wave height, which represents the secondary variable. Differently from the distribution for the primary variable, the secondary variable gives a more direct feeling of the sea encountered by the ship during the straight advancing: the most probable wave height is about 44 mm.

In Fig. 12 the PDF and the quantile function for the resistance are reported. The distributions are referred to the signal where the non-inertia effects, due to a relatively small surge motion, are subtracted. In principle the surge motion should be constrained, but it would be possible only with an infinitely rigid transversal beam, so that it remains

unrealistic. Non-inertial effects are estimated by assuming the added mass contribution equal to the 10% of the ship model mass; the apparent force term is then $1.1\Delta d\eta_1/dt$ where η_1 represents the surge motion (acquired by the Kripton system) and Δ is displacement defined in Table 1.

PDFs and quantiles for Heave and Pitch motions are reported in Fig. 13 and Fig. 14, whereas the ones for the Flight Deck velocity and the Bridge acceleration are in Fig. 15. Validation for resistance, heave, pitch, bridge acceleration and flight deck velocity time series, assessed with the various methods described in Diez et al. (2018b), are reported in Table 8, Table 9 and Table 10 for primary variables and in Table 11 for secondary variables.

In order to normalize the results, the uncertainties are expressed in percentage of $2SD$. Since the process $J(t)$ is assumed to be stationary, its autocovariance function depends only on the difference in time (time lag) between the two points. Following Belenky et al. (2015), it is useful to stress that, while the term (8) in formula (7) represents the variance of the mean estimate of a random variable, the term (9) highlights, in turn, the dependence between the data points of a stochastic process.

If the process may be assumed as an uncorrelated white noise, the result is identical to a random variable one, because the auto-covariance function of the white noise equals zero for all non-zero time lags.

Table 7

Irregular wave statistical analysis and uncertainty estimate by Autocovariance, Non-Overlapping Block Bootstrap, Moving Block Bootstrap methods for primary variable and Bootstrap Method for secondary variable.

Method	EV		SD		Quantile		Aver. absolute	
	E	U	E	U	E	U	E	U
Wave elevation (Primary)	AC	-1.65%	0.76%	-0.74%	1.65%	-	1.20%	1.21%
	NBB	-1.65%	1.05%	-0.84%	2.54%	2.13%	3.01%	5.31%
	MBB	-1.68%	1.20%	-0.80%	1.92%	2.10%	2.77%	5.30%
Wave height (Secondary)	BM	-6.62%	5.52%	-2.53%	4.9%	6.95%	8.09%	4.62%

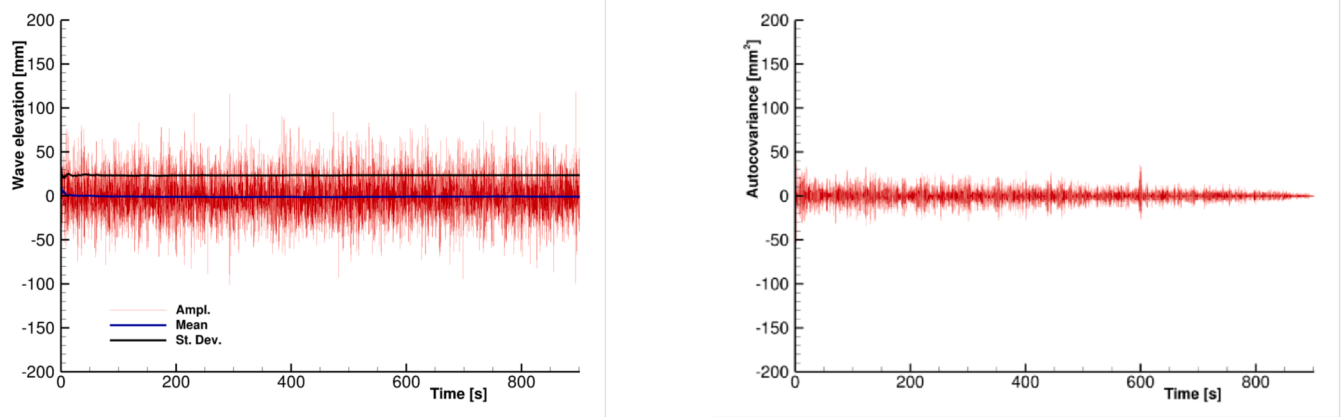


Fig. 10. Convergence of wave elevation EV and SD (Left) and autocovariance function (Right).

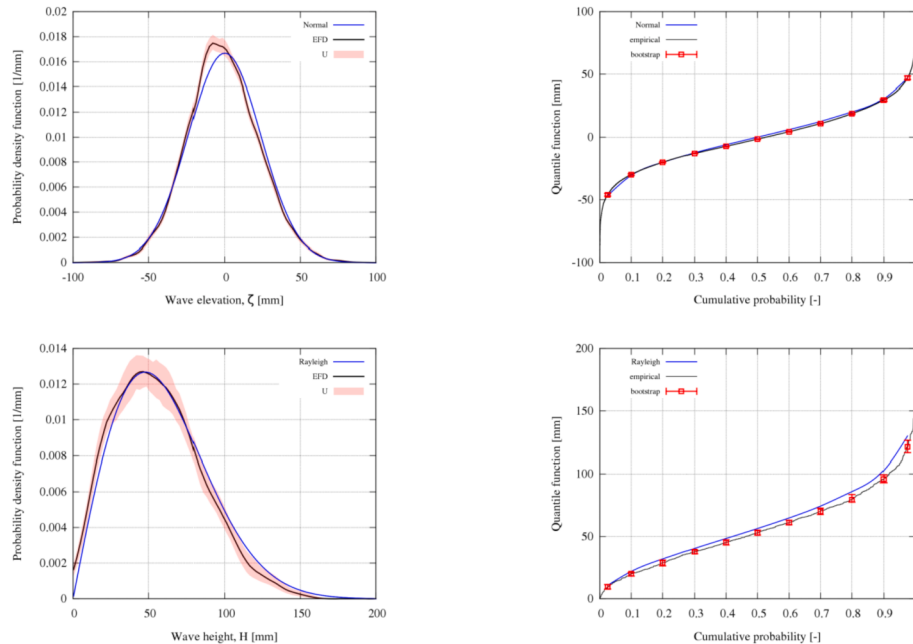


Fig. 11. Probability density function (Left) and Quantile function (Right) for wave elevation. On the top row the primary variable, on the bottom row the same functions for the secondary variable.

From Table 8, the low values of the uncertainties on the mean values reflect low variances on diagonal and off-diagonal terms, being equation (7) a sum of two positive terms: the first one goes to zero for the number of items going to infinity, whereas the second one goes to a stationary value. This means that, by enriching the items with longer time histories, the autocovariance function remains unaltered whereas the variance of the mean value becomes negligible, thus allowing to conclude that the process is stationary in a statistical sense.

Being the autocovariance analysis naturally biased by the order with which the different records are collected, the NBB and MBB methods, where the total signals are divided in bootstrapped series and rearranged, have been also considered. Table 8, Tables 9 and 10 show low and similar uncertainties both for the primary variables and for their standard deviations, this meaning that the experimental acquisitions are long enough to be unaffected by their collection. Conversely, the uncertainties associated to the secondary variables, evaluated with bootstrap method, are slightly larger although lower than the 3%. The quantiles of the secondary variables are affected by greater uncertainties, as indicated by Table 11 and detectable by Figs. 13, Figs. 14 and 15.

It should be finally stressed that the non-zero time averaged value of the flight deck velocity comes from a trivial error on the bridge acceleration integration that may be assumed negligible.

4.2. Regular wave tests

For the assessment of the stochastic regular wave UQ, a set of sea-keeping tests in regular waves has been performed. During the tests, the wave amplitude, the heave, the pitch and the resistance are recorded. Once the signals are acquired, their time average is computed and subtracted from the original signal; a Fourier transform is performed in order to check that the signals energies are confined in a narrow band around the first harmonic. The module of the associated Fourier (complex) coefficient is taken as representative value at the corresponding frequency.

The set of regular waves should be representative of the irregular wave campaign, *i.e.* of the benchmark. To this aim, a test matrix consisting of 33 monochromatic progressive waves with constant height equal to the mean wave height ($H_m = 61.1\text{mm}$, see Table 4) and frequencies uniformly distributed over the encounter frequencies interval

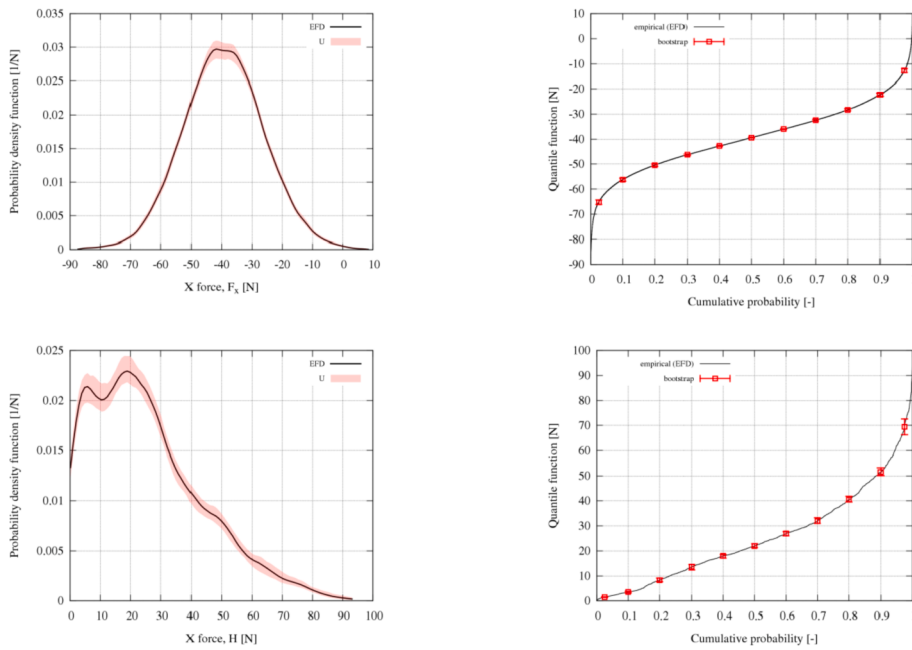


Fig. 12. Probability density function (Left) and Quantile function (Right) for X-force. On the top row the primary variable, on the bottom row the same functions for the secondary variable.

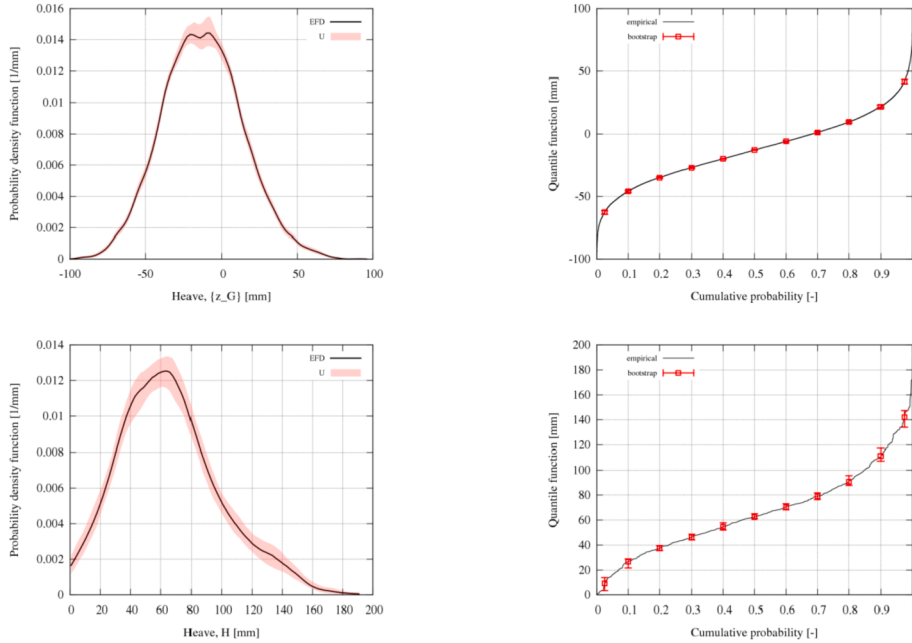


Fig. 13. Probability density function (Left) and Quantile function (Right) for Heave motion. On the top row the primary variable, on the bottom row the same functions for the secondary variable.

of the irregular wave is designed. The resulting test matrix is summarized in Table 12; the run 16 (in red), which is relative to a frequency near the heave peak, has been repeated for six times in order to assess the repeatability in the worst condition.

In Table 12 the wave steepness of the incident wave are reported as well; it has to be highlighted that, the range of frequencies/wave steepness considered is within the region of low error (max 5.5%) and low uncertainty (4%) of the wave maker operability (Table 2). However, to increase the confidence on the generated wave, the wave height has been measured at each run by the Kenek fixed on the carriage, placed 3 m ahead the catamaran. The Fourier transform of the signals allows to

evaluate the amplitude of the first harmonics, as well as of higher order harmonics (which should be negligible).

The measurements are reported in the plots of Fig. 16; first harmonics of the incident waves are reported in the left plot with square symbols, whereas the red line represents the desired value. As expected (thus confirming the validation assessment of the wave maker reported in section 2.3), the amplitudes of the generated waves show a satisfactory agreement with the desiderated value. The percentage errors (blue line in the left plot of figure) respect to the desired amplitude A_0 (30.55 mm) is everywhere lower than the 4%, although increasing with frequency.

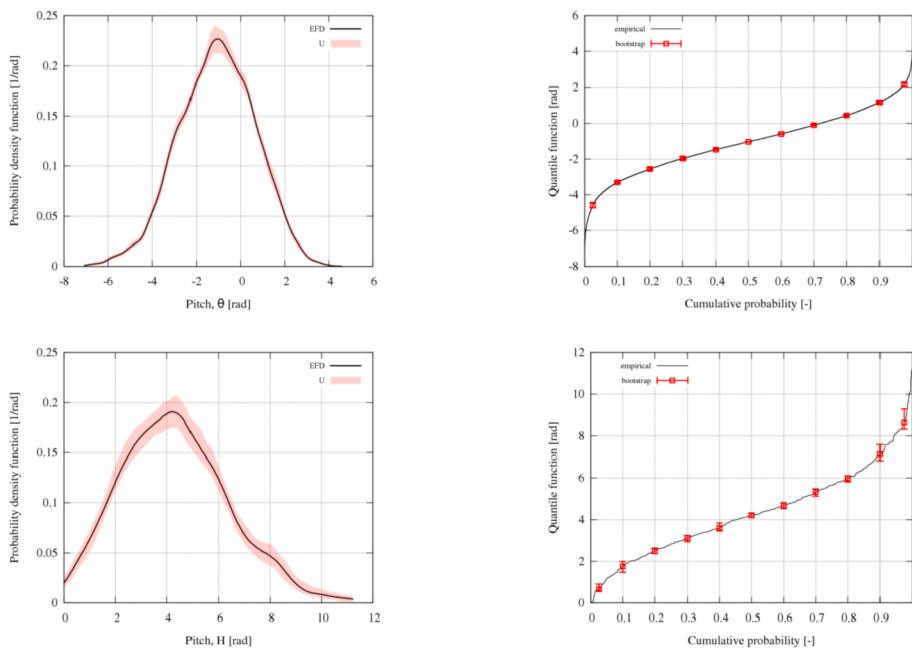


Fig. 14. Probability density function (Left) and Quantile function (Right) for Pitch motion. On the top row the primary variable, on the bottom row the same functions for the secondary variable.

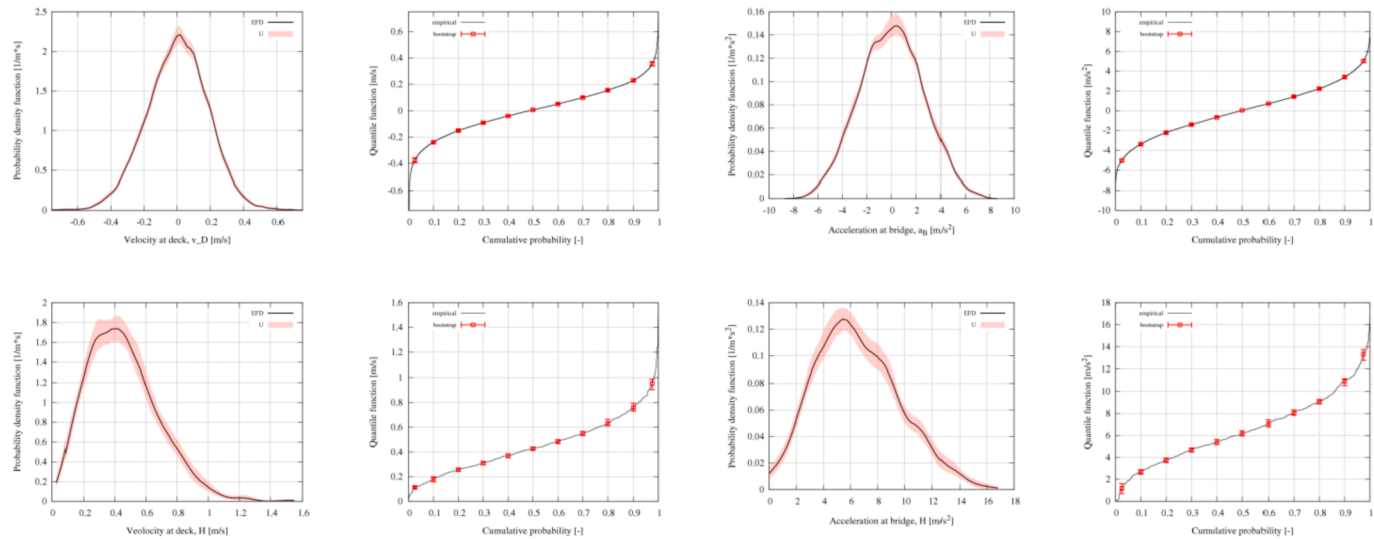


Fig. 15. Probability density function and Quantile function for Flight Deck Velocity (Left) and Acceleration (Right). On the top row the primary variables, on the bottom row the same functions for the secondary variables.

Table 8

EV, SD, and statistical uncertainties by time series and AC analysis for **primary variables**. Note that the uncertainties are %2SD.

Dim.		Mean		SD	
		Value	U	Value	U
Resistance	N	-39.31	0.97%	13.33	1.86%
Heave	mm	-12.38	0.68%	26.62	2.47%
Pitch	deg.	-1.07	0.32%	1.74	2.48%
Br. Acc.	m/s ²	0.01	0.05%	2.59	2.64%
FD. Vel.	m/s	0.00	0.26%	0.19	2.10%
Average			0.46%		2.31%

Table 9

EV, SD, Quantile and statistical uncertainties by NBB for **primary variables**. Note that the uncertainties are %2SD.

Dim.		Mean		SD		Quantile	
		Value	U	Value	U	Value	U
Resistance	N	-39.30	0.60%	13.35	1.55%	1.68%	
Heave	mm	-12.39	0.57%	26.58	1.53%	1.84%	
Pitch	deg.	-1.07	0.47%	1.74	1.19%	1.60%	
Br. Acc.	m/s ²	0.01	0.17%	2.60	1.28%	1.53%	
FD. Vel.	m/s	0.00	1.03%	0.19	1.76%	2.04%	
Average			0.57%		1.46%	1.74%	

Table 10

EV, SD, Quantile and statistical uncertainties by MBB for primary variables. Note that the uncertainties are %2SD.

	Dim.	Mean		SD		Quantile	
		Value	U	Value	U	Value	U
Resistance	N	-39.30	0.53%	13.34	1.41%	1.70%	
Heave	mm	-12.40	0.59%	26.59	1.29%	1.67%	
Pitch	deg.	-1.07	0.47%	1.74	1.07%	1.63%	
Br. Acc.	m/s ²	0.01	0.18%	2.60	1.44%	1.67%	
FD. Vel.	m/s	0.00	0.90%	0.19	1.91%	2.05%	
Average				1.07%	2.85%	1.74%	

Table 11

EV, SD, Quantile and statistical uncertainties by BM for secondary variables. Note that the uncertainties are %2SD.

	Dim.	Mean		SD		Quantile	
		Value	U	Value	U	Value	U
Resistance	N	25.37	1.88%	18.39	1.39%	2.85%	
Heave	mm	65.67	3.13%	33.11	2.41%	5.26%	
Pitch	deg.	4.30	3.04%	2.08	2.16%	5.07%	
Br. Acc.	m/s ²	6.48	2.82%	3.10	2.09%	4.49%	
FD. Vel.	m/s	0.45	2.48%	0.23	2.33%	4.23%	
Average				2.67%	2.08%	4.38%	

A mean value of 1.4% is found on average over the whole frequency range, thus remaining under the threshold of 5%, assumed by the ITTC standards (Load and Responses Commit, 2002) as a requirement. In order to evaluate the linearity of the generated waves, the second harmonics are also estimated and reported in the right frame of Fig. 16: the amplitudes are all less than 2 mm, with an average value over the frequency range less than 1 mm (solid red line), which corresponds to about the 3.0% of A_0 .

4.2.1. Calm water resistance

During the seakeeping tests, the hull resistance is measured through the load cells described in section 2.2; for every run performed, the first half of the basin is traveled in calm water, whereas in the second half regular waves are encountered; the calm water component is recorded every run and may be exploited for an estimation of the repeatability of the experiments in terms of steady force measurements. For each run, calm water resistances are reported in the left frame of Fig. 17 with a mean value of 32.8N: on the abscissa the wave frequency related to the corresponding run number is indicated. The results highlight a satisfactory repeatability for the resistance measurement with a mean percentage deviation from the average value of 1.2%. Fig. 17 shows (right panel) the mean error with a red line, while with blue dots the

percentage deviations of single runs are reported. A maximum deviation of 3.8% ensures a narrow error band. It is worth to remark that this result is comparable with the repeatability of the wave generation, discussed above, ensuring the reliability of all the facilities/instrumentations equipment.

4.2.2. In wave measurements

In Fig. 18 the Mean, Amplitude, RMS and Phase shift for Heave, Pitch, Resistance, Bridge acceleration and Flight Deck velocity (in dimensional form) versus the non-dimensional wavelength are shown. The peak on the Bridge acceleration amplitude (6.33m/s^2) is recorded in correspondence of $\lambda/L_{pp} \sim 1.1$, where the maximum in the heave motion (59.43 mm) appears, while the maximum of the flight deck velocity (0.38 m/s) is little anticipated at $\lambda/L_{pp} \sim 1.08$. For the sake of completeness, in Table 13, the lowest, the medium and the highest natural frequency cases (from left to right, respectively) are reported.

As it can be observed, the second harmonics amplitudes are always negligible compared to the first harmonics ones. In the experiment at $f = 0.6323\text{Hz}$ (at the heave peak), the second harmonics amplitude of the resistance is equal to the 24.5% of the first harmonics (whereas, at the lowest frequency, only the 0.8%), revealing a modulation in the load cell response due to the intense heave motion. Generally, the second harmonics components of heave, pitch and bridge acceleration are rather negligible until $f = 0.8758\text{Hz}$, where the wavemaker experiences some problem in generating linear monochromatic waves. Conversely, the resistance results more affected by a significant nonlinearity response, with greater amplitudes in the second harmonics components (up to the 80% of the first harmonics).

The RAO of heave and pitch (ξ_3/A and ξ_5/kA , respectively) are compared with those available literature on the top row of Fig. 20, whereas the phase shifts respect to the phases of the incoming waves are indicated in the bottom: the comparisons seem to be in good agreement. A repeatability analysis has been assessed at frequency of 0.6526Hz (i.e. $\lambda/L_{pp} \approx 1.22$, run 16 in Table 12); the chosen frequency corresponds to a condition close to the heave peak. Repeatability has been estimated through 6 repetitions. Results are summarized in Table 14. Satisfactory repeatability properties are seen for all the variables measured, being the standard deviation lower than the 1%, thus assessing a well restraint of the random errors.

In Fig. 21 the non-dimensional added resistance:

$$R_{aw} = \frac{R_w - R_c}{\rho A^2 g (2b)^2 / L_{pp}} \quad (37)$$

where R_w and R_c are the in wave (mean) and calm water resistances, is sketched versus the encounter frequency (left frame) and compared with the data available in literature (right frame).

Table 12

Regular waves, wave frequency is computed considering finite depth water with $h = 3.6m$.

Run	f [Hz]	f _e [Hz]	λ [m]	H_m/λ	κA	λ/L_{pp}	17	0.6323	1.2228	3.9038	0.0157	0.0492	1.3013
1	0.9569	2.3093	1.7045	0.0358	0.1126	0.5682	18	0.6121	1.1654	4.1656	0.0147	0.0461	1.3885
2	0.9360	2.2323	1.779	0.0343	0.1079	0.5931	19	0.5918	1.1091	4.4561	0.0137	0.0431	1.4854
3	0.9164	2.1567	1.8585	0.0329	0.1033	0.6195	20	0.5715	1.0539	4.7779	0.0128	0.0402	1.5926
4	0.8961	2.0821	1.9437	0.0314	0.0988	0.6479	21	0.5512	1.0001	5.1356	0.0119	0.0374	1.7119
5	0.8758	2.0086	2.048	0.0300	0.0943	0.6783	22	0.5309	0.9474	5.5344	0.0110	0.0347	1.8448
6	0.8555	1.93	2.11	0.0287	0.0900	0.7109	23	0.5106	0.8961	5.9804	0.0102	0.0321	1.9935
7	0.8352	1.8655	2.2375	0.0273	0.0858	0.7458	24	0.4903	0.8460	6.4805	0.0094	0.0296	2.1602
8	0.8149	1.7957	2.3503	0.0260	0.0817	0.7834	25	0.4700	0.7974	7.0426	0.0087	0.0273	2.3475
9	0.7946	1.7272	2.4720	0.0247	0.0776	0.8240	26	0.4498	0.7502	7.6721	0.0080	0.0250	2.5574
10	0.7743	1.6598	2.6033	0.0235	0.0737	0.8678	27	0.4295	0.7044	8.3844	0.0073	0.0229	2.7948
11	0.7541	1.5940	2.7446	0.0223	0.0699	0.9149	28	0.4092	0.6601	9.1867	0.0067	0.0209	3.0622
12	0.7338	1.5291	2.8986	0.0211	0.0662	0.9662	29	0.3889	0.6174	10.0892	0.0061	0.0190	3.3631
13	0.7135	1.4654	3.0659	0.0199	0.0626	1.0220	30	0.3686	0.5762	11.1035	0.0055	0.0173	3.7012
14	0.6932	1.4029	3.2481	0.0188	0.0591	1.0827	31	0.3483	0.5366	12.2421	0.0050	0.0157	4.0807
15	0.6729	1.3417	3.4470	0.0177	0.0557	1.1490	32	0.3280	0.4985	13.5203	0.0045	0.0142	4.5068
16	0.6526	1.2816	3.6647	0.0167	0.0524	1.2216	33	0.3077	0.4619	14.9574	0.0041	0.0128	4.9858

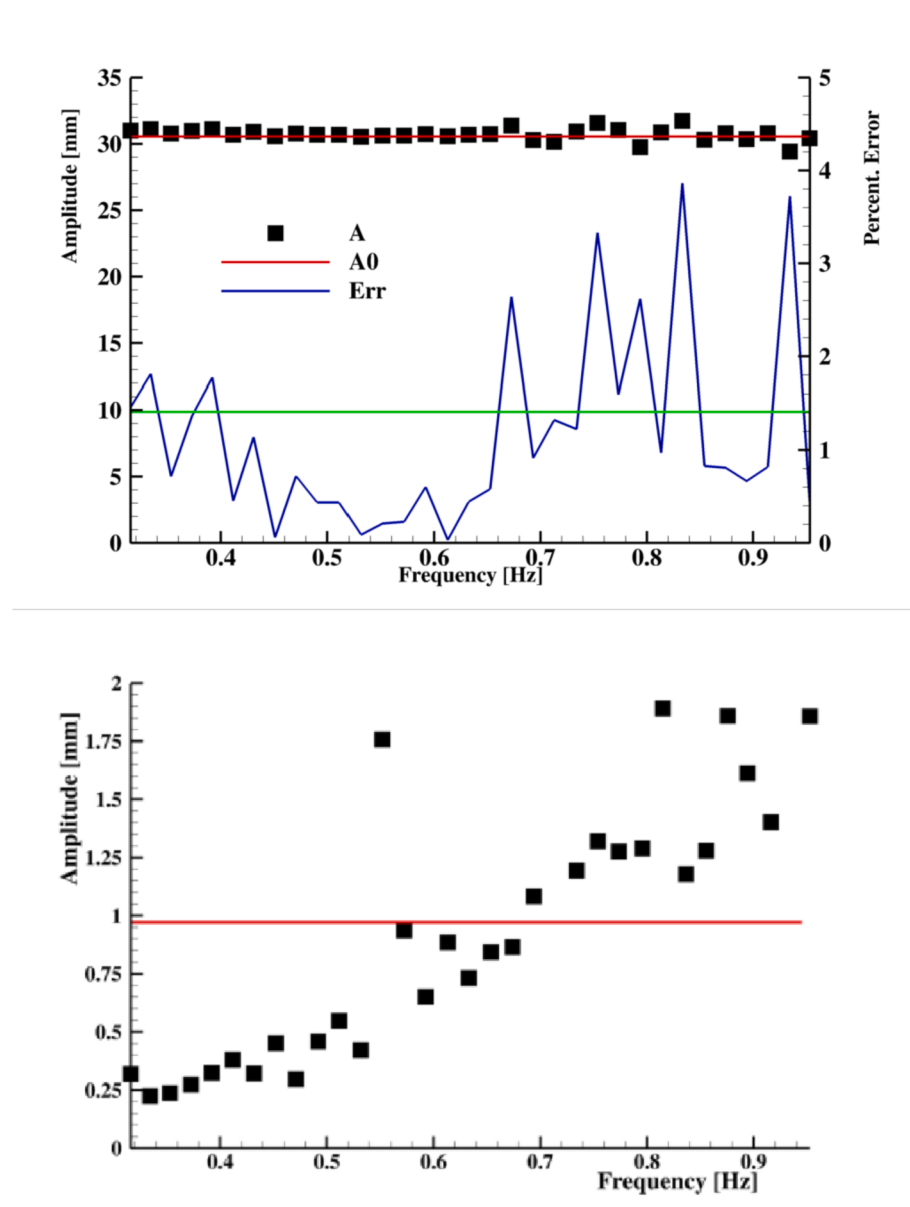


Fig. 16. Left: Amplitudes (in mm) of the waves generated versus frequencies. In red the desired amplitude. In blue the percentage error. In green the mean percentage error. Right: Second harmonics components of the wave amplitudes. In red the mean value.

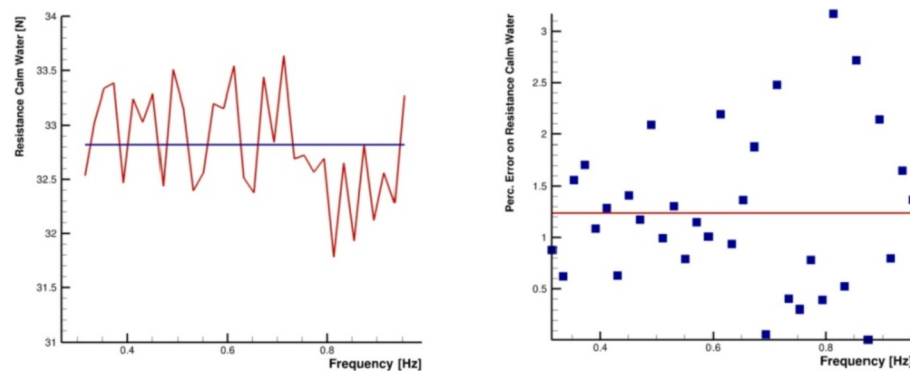


Fig. 17. Left: Mean calm water resistance (blue) and related values (red) respect to the run number. Right: Percentage error in amplitude (blue dots) respect to the run number (expressed with the corresponding frequency). In red the mean error.

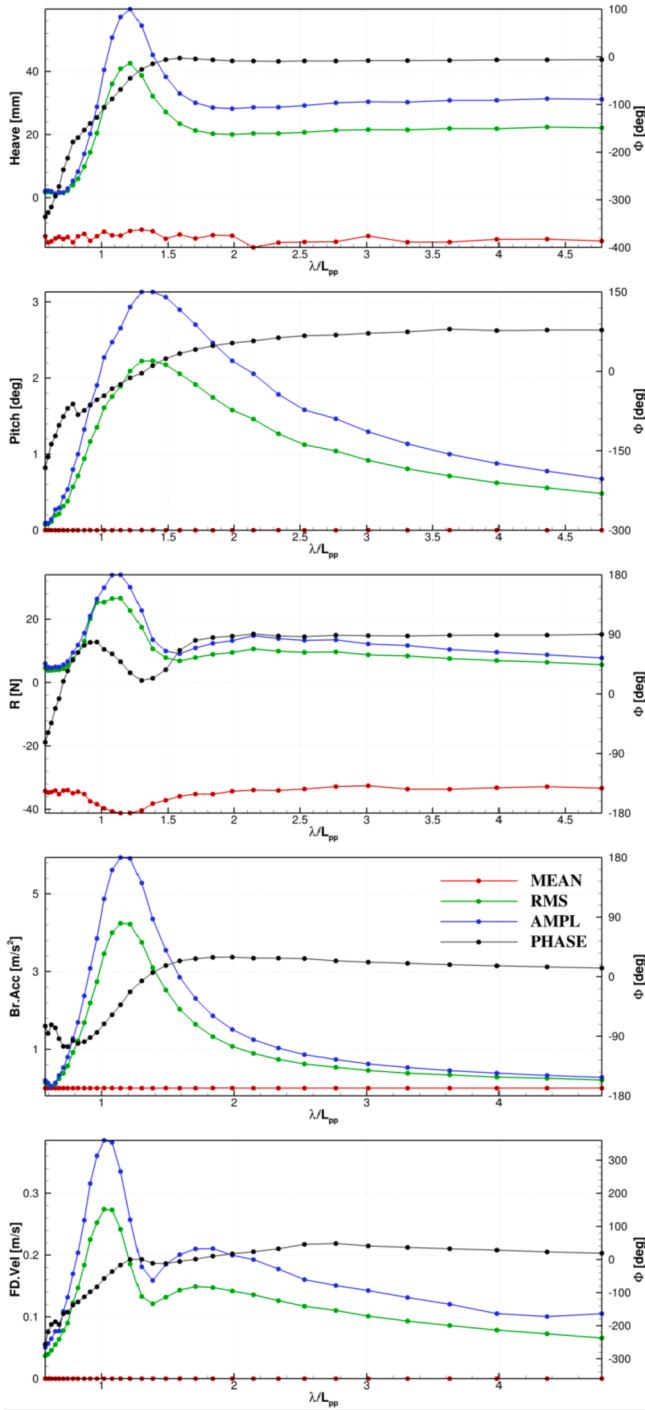


Fig. 18. From top to bottom: Amplitude (blue), Mean (red), RMS (green) and Phase shift (black) for Heave, Pitch, Resistance, Bridge acceleration and Flight Deck velocity, respectively, versus non-dimensional wave length.

For high frequencies and short wave lengths, the added resistance is caused by the wave diffraction and becomes rather constant ($R_{aw} \sim 2$), whereas, at longer wave lengths and low frequencies, the radiation is the dominant effect. At the latter conditions, R_{aw} becomes negligible for λ/L_{pp} high enough, approaching the total resistance to calm water condition. At the present Froude number, a negligible added resistance is found for $\lambda/L_{pp} > 2.5$.

The peak of the added resistance occurs at $\lambda/L_{pp} \sim 1.17$ and it represents a condition of generation of large waves in the vicinity of resonant heave and pitch of the system due to an encounter frequency around

1.30 Hz. The corresponding non-dimensional wave length is about 1.16, related to a peak $R_{aw} \sim 12$ which is in good agreement with experiments discussed in (He et al., 2013), as shown in the right frame of Fig. 21, where the peaks for different Froude numbers are in the wave-length range λ/L_{pp} between 1 and 1.5 and the corresponding amplitudes span from 7.5 to 17. As evident, the added resistance peaks move toward lower values of λ/L_{pp} as the *Fr* number decreases: in the present case, the peak is very close to the one of Castiglione et al. (2011) for *Fr* = 0.45 which is close to the *Fr* = 0.425 used for the present experiments. As visible from the same figure, the short and long length behaviors are in accordance with the literature. Under the hypothesis of linear behavior (*i.e.* small motions) and uncoupled ship motions, the response of a ship in waves can be mathematically described by the classical second order (forced) mass, springer and damper system (see (Lewis, 1989), (Lloyd, 1989)).

Therefore, the theoretical natural frequencies for heave f_{n3} and pitch f_{n5} can be simply derived considering the homogenous system (*i.e.* with zero external force); if heave added mass and pitch added inertia are assumed to be equal to the mass m and the pitch moment of inertia I_{55} , respectively, natural frequencies can be computed as

$$f_{n3} = \sqrt{gC_{WP}/8\pi^2 C_B T} \quad f_{n5} = \sqrt{\rho g C_{IT}(2b)^3 L_{PP}/96\pi^2 I_{55}} \quad (38)$$

where $C_{WP} = A_W/(2b) L_{pp}$ is the water plane coefficient, $C_B = \Delta/2bL_{pp}T$ is the block coefficient (Δ is the volume of fluid displaced), and $C_{IT} = 12 I_T/(2b)^3 L_{pp}$ is the coefficient of inertia of the water plane area about the y axis. A_W denotes the water plane area of the hull and I_T its moment of inertia; these quantities can be computed from the hydrostatics characteristics of the model, giving $A_W = 1.093 \text{ m}^2$ and $I_T = 0.589 \text{ m}^4$. The quantities $\rho g A_W$ and $\rho g I_T$ are respectively the restoring heave force and pitch torque. Under the cited assumption, natural heave and pitch frequencies are estimated to be $f_{n3} = 1.27 \text{ Hz}$ and $f_{n5} = 1.17 \text{ Hz}$, respectively. As remarked by Lewis (1989), the natural frequency does not depend on the Froude number. Moreover, it is important to note that these estimations were developed for mono-hull displacement vessels and their validity for high speed (semi-displacement) multihulls is still an open issue. At a given Froude, the frequency at which maximal motion occurs ranges between the resonance one and that of maximal excitation forces/momenta. Lewis (1989) showed that a non-dimensional heave excitation force goes to unity for low frequencies, whereas the dimensional pitch excitation moment has a peak for the ratio $\lambda/L_{pp} = 1.33$.

In the present investigation, an heave peak is observed at $\lambda/L_{pp} \sim 1.22$ and a pitch peak at $\lambda/L_{pp} \sim 1.45$, as may be observed in Fig. 19; for low encounter frequencies the non-dimensional heave and pitch tend to unity (in agreement with (Lewis, 1989)), whereas for high frequencies the hulls motions are practically indifferent to the presence of short length waves and consequently the heave and the pitch become negligible.

4.2.3. Effect of the mounting system

The mounting system used for towing the catamaran, described in section 2.1, is now briefly discussed in terms of the effects on the added resistance. As shown in Fig. 22 the use of soft springs in the mounting system does not alter the RAO's of heave and pitch (see bottom frames in Fig. 22), while it affects significantly the resistance of the catamaran. With the first-designed system the mounting was not enough rigid, so that the elastic response of the beam induced an over-prediction of the ship resistance in the frequency range near the maximum of the heave (about 0.65 Hz). The first harmonics shown in the top-right frame of Fig. 22 highlights this aspect more clearly. The new mounting system is more rigid than the former one and is designed to be used with or without additional springs. Fig. 22 shows the effect when soft springs are used: an excessive filtering is visible through an under-prediction of the added resistance (although heave and pitch RAOS are unaffected) and a negligible amplitude in the 1st harmonics component. It has to be

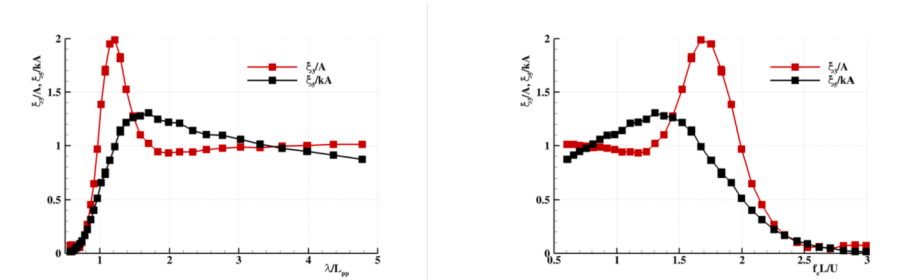


Fig. 19. Non-dimensional heave and pitch respect to non-dimensional wave length (left) and respect to non-dimensional encounter frequency (right).

Table 13

Mean, RMS (σ), 1st and 2nd harmonics Amplitude for three selected frequencies.

	$f = 0.3077 \text{ Hz}$				$f = 0.6323 \text{ Hz}$				$f = 0.9569 \text{ Hz}$			
	Mean	σ	A	A 2nd	Mean	σ	A	A 2nd	Mean	σ	A	A 2nd
Heave [mm]	-13.72	22.13	31.17	0.543	-10.11	38.72	54.51	0.151	-12.23	1.79	2.13	0.300
Pitch [deg]	0.00	0.48	0.67	0.034	0.00	2.22	3.13	0.059	0.00	0.07	0.09	0.014
Br. Acc [m/s^2]	0.00	0.21	0.27	0.023	0.00	3.75	5.28	0.198	0.00	0.15	0.20	0.011
FD.Vel [m/s]	0.00	0.06	0.10	0.015	0.00	0.13	0.18	0.022	0.00	0.04	0.05	0.003
R [N]	-33.32	5.65	7.75	0.062	-40.35	17.47	22.74	5.571	-34.21	4.62	5.99	1.095

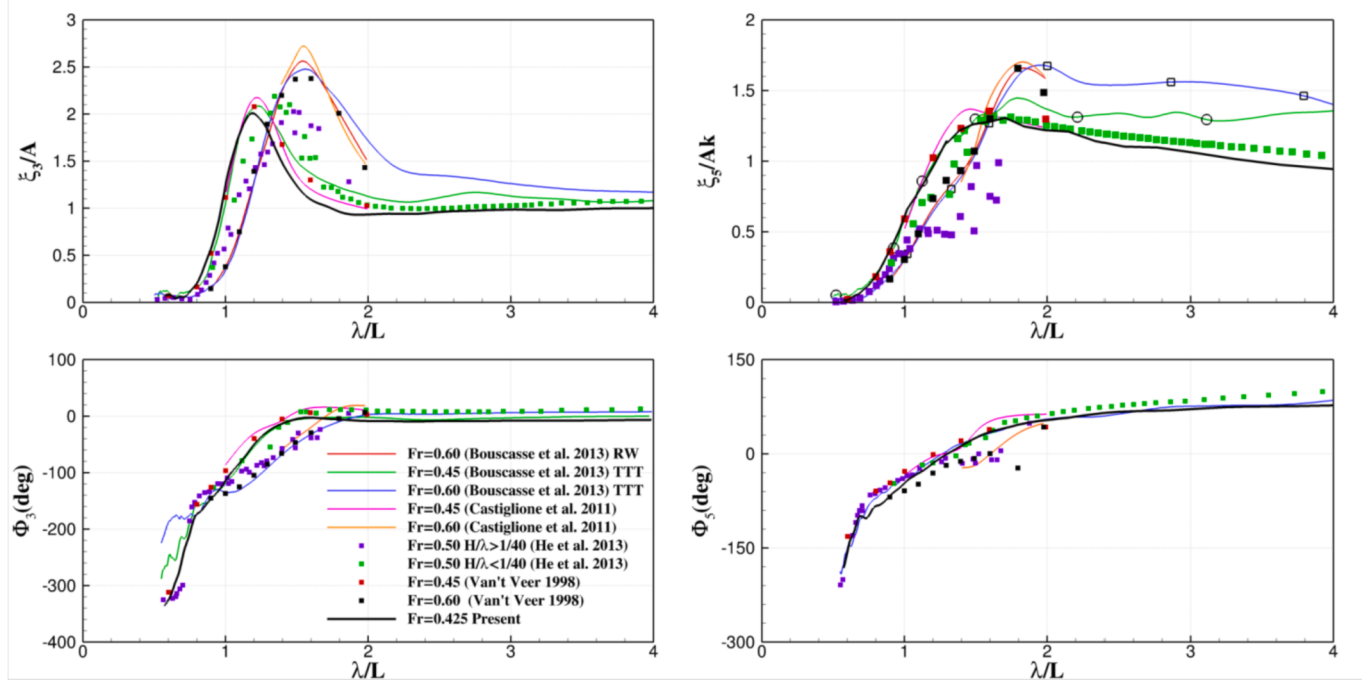


Fig. 20. Comparisons of the heave and pitch RAOS with the Literature ones. On the left column the non-dimensional heave (top) and pitch (bottom). On the right the corresponding phase shifts. The quantities are drawn respect to the non-dimensional wave-length with red line and black dots. TTT stands for Transient Test Technique, RW for Regular Wave tests; for details see [3].

Table 14

Repeatability for Pitch, Heave and in wave resistance R_w .

Run	1	2	3	4	5	6	X_M	RMS[% X_M]
Heave [mm]	-19.605	-19.739	-19.624	-19.857	-19.274	-19.388	-19.58	0.4%
Pitch [deg]	1.025	1.031	1.035	1.027	1.012	1.020	1.026	0.3%
R_w [N]	-41.27	-41.12	-41.96	-41.02	-41.52	-42.25	-41.53	0.4%

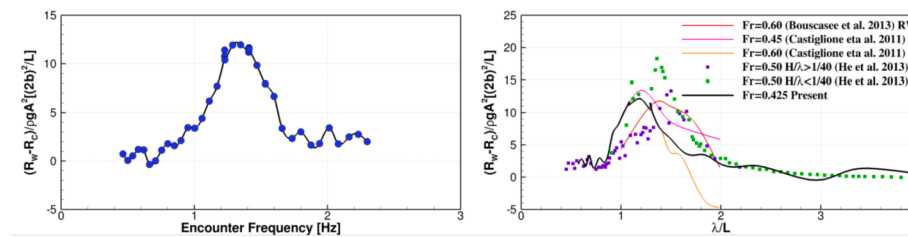


Fig. 21. Left: Non-dimensional added resistance respect to encounter frequency: experimental outputs. Right: comparisons with available Literature (black line with blue circles).

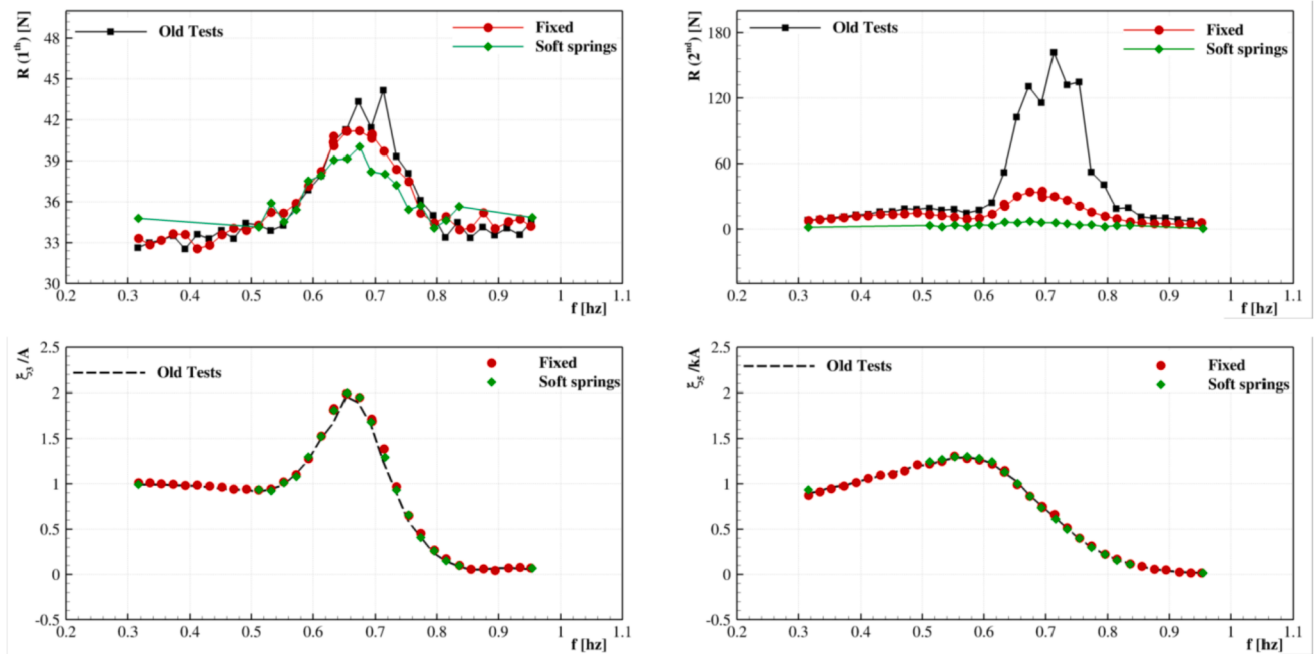


Fig. 22. Top Left: added resistance comparisons respect to wave frequency – 0th harmonics. Top Right: added resistance comparisons respect to wave frequency – 1st harmonics. Bottom left: heave comparisons. Bottom Right: pitch comparisons.

highlighted that, even if the use of soft springs could be ideal for added resistance prediction, it is not possible to use them for the current purposes, since for an uncertainty quantification assessment estimation of the first order harmonic is required. Several springs with different stiffness have been tested, revealing that soft springs are more effective in their filtering action, being the stiffer ones scarcely distinguishable by

the rigid arrangement.

4.3. Regular wave model

The set of 33 regular wave tests, equally spaced in encounter frequency and indicated in Section 4.2, has been adopted as training set for

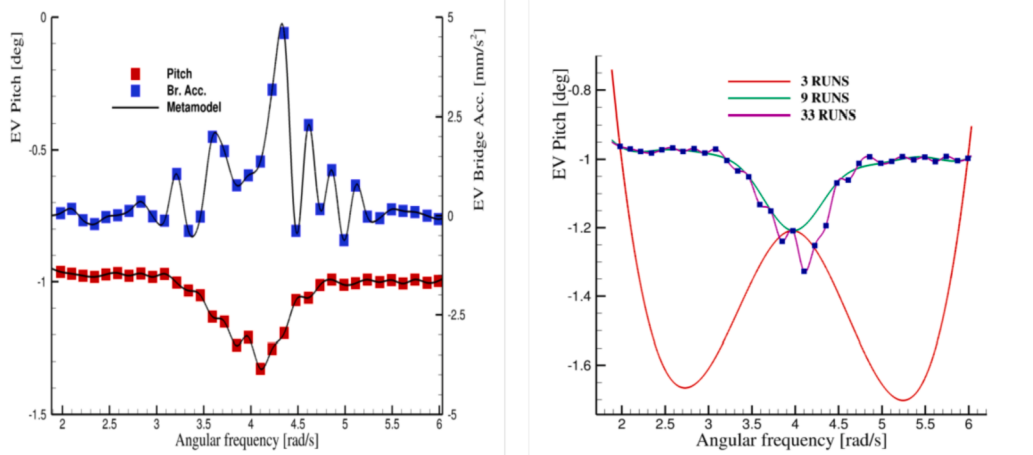


Fig. 23. Left: Examples of meta-models predictions for pitch and bridge acceleration. Right: meta-model convergence for EV of pitch angle.

Table 15
Regular wave UQ for SSAs.

Method	SSA	Unit	Value	$U_{\text{SSA}}\% \text{SSA}$	Regular VS Irregular
Irregular	θ	deg	3.48	2.47	
		m/s^2	5.19	2.63	
		m/s	0.36	3.72	
Regular	θ	Average		2.94	
		deg	3.73	9.54	+ 7.18%
		m/s^2	5.70	9.54	+ 9.83%
	θ	m/s	0.39	9.54	+ 8.33%
		Average			8.45%

the UQ meta-model. The test responses are evaluated in terms of heave and pitch RAOs, shown in Fig. 19, whereas the pitch, the bridge acceleration and the flight deck velocity are used as training set for the definition of the meta-model. The expected value $EV_i(J)$ and the standard deviation $SD_i(J)$ indicated in equation (29) are estimated through spline interpolator as sketched in the left plot of Fig. 23.

The evaluation of the SSA is outlined in Table 15, where is evident that the irregular and regular tests present a good agreement with a mean error under 10% and a maximum error on the bridge acceleration around the 9.8%. Conversely, the deterministic regular wave model, calculated through formula (26), is used to evaluate the expected value of the resistance, which is -37.85N with a difference of +3.71% with respect to the irregular case.

The uncertainties indicated in Table 15 for the regular case are calculated with the autocovariance method (equation (16)) without considering the non-diagonal terms in the autocovariance matrix. This leads to a value independent by the specific SSA value and only depends on the total number of items.

In order to highlight the effect given by the increasing of wave frequencies in the training set, needed for an acceptable meta-model prediction, the convergence of the interpolation curves in terms of expected value of the pitch angle is sketched in the right plot of Fig. 23. In Table 16, the SSAs convergence for the pitch angle, the bridge acceleration and the flight deck velocity are also shown: the pitch angle and the flight deck velocity exhibit a rather fast convergence with an achievement of the final value with just 9 runs. Conversely, the bridge acceleration shows a slower trend with a 27% of variation between 17 and 33 runs.

The comparison between regular and irregular tests in terms of heave and pitch RAO's is depicted in Fig. 24. Being the RAO a simplified statistic used to predict the heave and pitch motions in a real sea state, it is of great interest to evaluate how this assumption is in agreement with the irregular wave experiments, even for the average sea state condition (SS5) of the present work. Something similar was investigated by Bouscasse et al. (2013), although for mild sea state conditions (SS2 and SS3) and a different energy density spectrum (Pierson Moskowitz).

From the figure is evident how the pitch RAO is in good agreement with the irregular tests in the whole range of frequencies of the incoming waves; conversely, the heave RAO is very well reproduced in the range [0.4–0.75] Hz, where the behaviour may be considered linear while the tests are in some disagreement for higher frequencies. In particular, the range of well agreement corresponds to an encounter frequency range of [0.6–1.7] Hz, where the added resistance presents its maximum. Concluding, at the present conditions the description of a formed sea

Table 16
SSAs convergence with the increasing of the regular wave runs.

N. Runs	Pitch [deg]	Br. acc. [m/s^2]	F.D. vel. [m/s]
3	5.61	1.96	0.13
5	3.72	2.04	0.19
9	3.71	2.76	0.31
17	3.72	4.15	0.38
33	3.73	5.70	0.39

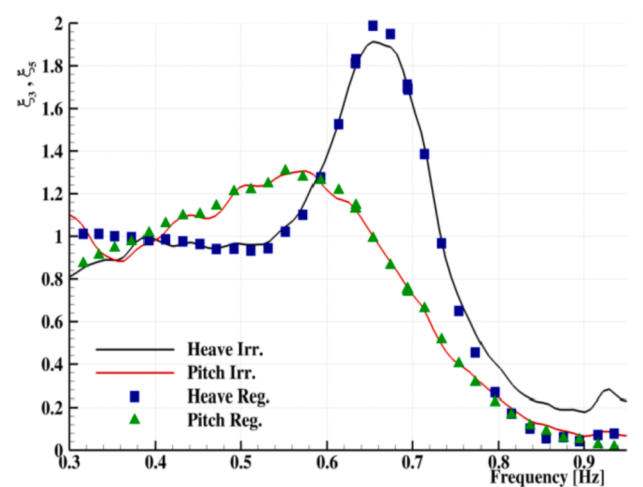


Fig. 24. Non-dimensional heave and pitch respect to wave angular frequency. With points the regular wave tests, with solid lines the Fourier transforms coming from the irregular wave experiments.

state through a set of regular waves is able to reproduce the heave and pitch RAO's as well as, through a meta-model, the SSA of the irregular wave experiments. In the framework of the numerical simulations, this aspect could be very important because it avoids the necessity to design a very fine grid for achieving a well resolved free surface when a real sea state is simulated. Conversely, a set of regular waves and the adoption of a metamodel, like the one described in the present work, are able to adequately describe the irregular wave sea condition.

5. Conclusions

A statistically-converged experimental benchmark study of a catamaran in irregular waves is presented, along with regular-wave uncertainty quantification (UQ) model used to approximate the relevant statistical estimators. The validation variables are x -force, z , θ , \dot{z}_B and \dot{z}_{FD} . Values from the time series are addressed as primary variables, whereas heights associated to mean-crossing waves are indicated as secondary variables.

A massive experimental campaign has been carried out with a great accuracy in the assessment of facilities and instrumentations reliabilities, thoroughly detailed in the present work. The global error due to the wave generations is well limited within the standard limit of 5%, as well as the instrumental errors in capturing the hull motions.

Different mounting systems have been tested; for the current analysis the system which ensures a rigid fix with the carriage, with negligible elastic reaction, has been demonstrated to be the more suitable.

The current approach addresses the statistics of the relevant variables, providing their EV, SD and their related uncertainties. The autocovariance and bootstrap methods are applied in order to estimate expected values and confidence intervals for EV, SD and quantile function. Additionally, the deterministic regular wave model assesses the EV of the x -force, whereas the stochastic regular wave UQ focuses on SSAs of θ , \dot{z}_B , and \dot{z}_{FD} , as relevant merit factors for design optimization.

At the current stage of the work, the discussion on which method provides the most realistic/appropriate validation uncertainty still remains open. On the one hand, the present implementation of the autocovariance and bootstrap methods has four main advantages: (1) uncertainties do not depend solely on the number of time steps, but also on the number of encountered waves (which is a real physical parameter and not an arbitrary implementation parameter); (2) it provides validation values and uncertainties not only for the time series EV and SD, but also distribution parameters (such as quantiles); (3) it can be applied not only to primary variables (time series) but also to secondary

variables (amplitudes, height, period); (4) it can detect possible stationarity issues in the time-series. The main drawback of the block bootstrap method is that the time series is not directly assessed for correlation. A second drawback is the assumption of independence of the sample required by the bootstrap method used for the secondary variables. On the other hand, the time series method has the main advantage of evaluating directly the EV and SD uncertainty stemming from the wave record dependence. As a drawback, it does not directly provide confidence intervals for other parameters than time series EV and SD, and does not address directly possible stationarity issues (at least when concatenated records are used). A combination of the two methods is therefore advisable.

Ongoing and future work will address a nested array approach. Possibly, the experiments will be also extended to a longer run length. The relationship of the overall validation uncertainty to both the number of wave components and the run length depends on the problem (sea state, spectrum, speed, geometry) and will be quantitatively investigated in future work, at least for current problem. U_{SN} and U_D will be included in the validation analysis. Additionally, EV and distribution error and uncertainty will be included in the assessment of the stochastic regular wave UQ model.

Acknowledgements

The present research is supported by the Office of Naval Research (grant N00014-14-1-0195) and Office of Naval Research Global (NICOP grant N62909-11-1-7011 and N62909-12-1-7082), under the administration of Dr. Ki-Han Kim and Dr. Woei-Min Lin.

References

- Belenky, V., Pipiras, V., Kent, C., Hughes, M., Campbell, B., Smith, T., 2013. On the statistical uncertainty of time-domain-based assessment of stability failure: confidence interval for the mean and the variance of a time series. In: Proc. 13th International Ship Stability Workshop, Brest, France, pp. 23–26 September.
- Belenky, V., Pipiras, V., Weems, K., 2015. Statistical uncertainty of ship motion data. In: Proc. 12th International Conference On the Stability Of Ships And Ocean Vehicles. STAB, Glasgow, UK, pp. 14–19. June.
- Bouscasse, B., Broglia, R., Stern, F., 2013. Experimental investigation of a fast catamaran in head waves. *Ocean Eng.* 72, 318–330.
- Broglia, R., Jacob, B., Zaghi, S., Stern, F., Olivieri, A., 2014. Experimental investigation of interference effects for high-speed catamarans. *Ocean Eng.* 76, 75–85.
- Broglia, R., Zaghi, S., Campana, E.F., Visonneau, M., Queutey, P., Dogan, T., Sadat-Hosseini, H., Stern, F., Milanov, E., 2015. CFD validation for DELFT 372 catamaran in static drift conditions, including onset and progression analysis. In: Proc. 5th World Maritime Technology Conference, Rhode Island, USA, pp. 3–7. November.
- Broglia, R., Zaghi, S., Campana, E.F., et al., 2019. Assessment of CFD capabilities for the prediction of three dimensional separated flows: the DELFT 372 catamaran in static drift conditions. ASME J. Fluids Eng. <https://doi.org/10.1115/1.4042752>.
- Carlstein, E., 1986. The use of subseries values for estimating the variance of a general statistic from a stationary sequence. *Ann. Stat.* 14 (3), 1171–1179.
- Castiglione, T., Stern, F., Bova, S., Kandasamy, M., 2011. Numerical investigation of the seakeeping behavior of a catamaran advancing in regular head waves. *Ocean Eng.* 38 (16), 1806–1822.
- Castiglione, T., He, W., Stern, F., Bova, S., 2014. URANS simulations of catamaran interference in shallow water. *J. Mar. Sci. Technol.* 19, 33–51. <https://doi.org/10.1007/s00773-013-0230-5>.
- Chen, X., Diez, M., Kandasamy, M., Campana, E.F., Stern, F., 2013. Design optimization of the waterjet-propelled Delft catamaran in calm water using URANS, design of experiments, metamodels and swarm intelligence. In: Proc. 12th International Conference on Fast Sea Transportation. FAST, Amsterdam, The Netherlands, pp. 2–5. December.
- Chen, X., Diez, M., Kandasamy, M., Zhang, Z., Campana, E.F., Stern, F., 2015. High-fidelity global optimization of shape design by dimensionality reduction, metamodels and deterministic particle swarm. *Eng. Optim.* 47 (4), 473–494.
- Diez, M., Chen, X., Campana, E.F., Stern, F., 2013. Reliability-based robust design optimization for ships in real ocean environment. In: Proc. 12th International Conference On Fast Sea Transportation. FAST, Amsterdam, The Netherlands, pp. 2–5. December.
- Diez, M., He, W., Campana, E.F., Stern, F., 2014. “Uncertainty quantification of Delft catamaran resistance, sinkage and trim for variable Froude number and geometry using metamodels, quadrature and Karhunen–Loève expansion”. *J. Mar. Sci. Technol.* 19 (2), 143–169.
- Diez, M., Campana, E.F., Stern, F., 2015. “Design-space dimensionality reduction in shape optimization by Karhunen–Loève expansion”. *Comput. Methods Appl. Mech. Eng.* 283, 1525–1544.
- Diez, M., Campana, E.F., Stern, F., 2018. Stochastic optimization methods for ship resistance and operational efficiency via CFD. *Struct. Multidiscip. Optim.* 57 (2), 735–758.
- Diez, M., Broglia, R., Durante, D., Olivieri, A., Campana, E.F., Stern, F., 2018. Statistical assessment and validation of experimental and computational ship response in irregular waves. *J. Verif., Validation, Uncertain. Quantification* 3 (2), 021004.
- Efron, B., 1981. Nonparametric estimates of standard error: the jackknife, the bootstrap and other methods. *Biometrika* 68 (3), 589–599.
- Falchi, M., Felli, M., Grizzi, S., Aloisio, G., Broglia, R., Stern, F., 2014. SPIV measurements around the DELFT 372 catamaran in steady drift. *Exp. Fluid* 55 (11).
- Faltinsen, O.M., 2005. Hydrodynamics of High-Speed Marine Vehicles. Cambridge University Press.
- Fu, T.C., Brucker, K.A., Mousaviraad, S.M., Ikeda, C.M., Lee, E.J., O’Shea, T.T., Wang, Z., Stern, F., Judge, C.Q., 2014. An assessment of computational fluid dynamics predictions of the hydrodynamics of high-speed planing craft in calm water and waves. In: Proc. 30th Symposium on Naval Hydrodynamics. Hobart, Tasmania, Australia, pp. 2–7. November.
- He, W., Diez, M., Zou, Z., Campana, E.F., Stern, F., 2013. URANS study of Delft catamaran total/added resistance, motions and slamming loads in head sea including irregular wave and uncertainty quantification for variable regular wave and geometry. *Ocean Eng.* 74, 189–217.
- He, W., Castiglione, T., Kandasamy, M., Stern, F., 2015. Numerical analysis of the interference effects on resistance, sinkage and trim of a fast catamaran. *J. Mar. Sci. Technol.* 20 (2), 292–308.
- Huang, J., Carrica, P., Stern, F., 2008. Semi-coupled air/water immersed boundary approach for curvilinear dynamic overset grids with application to ship hydrodynamics. *Int. J. Numer. Methods Fluids* 58, 591–624.
- Kennell, C.G., White, B.L., Comstock, E.N., 1985. Innovative naval designs for North Atlantic operations. *SNAME Trans.* 93, 261–281.
- Künsch, H.R., 1989. The jackknife and the bootstrap for general stationary observations. *Ann. Stat.* 17, 1217–1241.
- Lewis, E.V., 1989. Principles of Naval Architecture. The Society of Naval Architects and Marine Engineers, New York.
- Lloyd, A.R.J.M., 1989. Seakeeping: Ship Behaviour in Rough Weather. Ellis Horwood Limited, Chichester, West Sussex.
- Load and responses committee of 23rd ITTC, “testing and extrapolation methods loads and responses, sea keeping experiments”. ITTC-Recommended Procedures 7, 2002, 5-02-07-02.1.
- Longo, J., Stern, F., 2005. Uncertainty assessment for towing tank tests with example for surface combatant DTMB model 5415*. *J. Ship Res.* 49, 55–68.
- Miecznikowski, J.C., Wang, D., Huston, A., 2010. Bootstrap MISE estimators to obtain bandwidth for kernel density estimation. *Comm. in Statistics-Simulation and Comp.* 39 (7), 1455–1469.
- Miecznikowski, J.C., Wang, D., Huston, A., 2010. Bootstrap MISE estimators to obtain bandwidth for kernel density estimation. *Commun. Stat. Simulat. Comput.* 39 (7), 1455–1469.
- Mollison, D., Evans, Falcão, 1985. In: Wave Climate and the Wave Power Resource. Hydrod. Of Ocean-Wave Energy Utilization”, *Proc. IUTAM Symp.*, pp. 133–156. Lisbon, Portugal.
- Mousaviraad, S.M., He, W., Diez, M., Stern, F., 2013. Framework for convergence and validation of stochastic uncertainty quantification and relationship to deterministic verification and validation. *Int. J. Uncertain. Quantification* 3, 5.
- Mousaviraad, S.M., Wang, Z., Stern, F., 2013. URANS studies of hydrodynamic performance and slamming loads on high-speed planing hulls in calm water and waves for deep and shallow conditions. In: Proc. Of the 3rd International Conference On Ship Manoeuvring In Shallow & Confined Water: Ship Behaviour In Locks, Ghent, Belgium, pp. 3–5. June.
- NATO STANAG 4154, 1997. Common Procedures in the Ship Design Process. Seakeeping Criteria for General Application (Chapter 7).
- Politis, D.N., Romano, J.P., 1994. The stationary bootstrap”. *J. Am. Stat. Assoc.* 89, 1303–1313.
- Politis, D.N., Romano, J.P., Wolf, M., 1999. Subsampling. Springer, New York.
- Sadat-Hosseini, H., Chen, X., Milanov, E., Stern, F., 2013. CFD and system-based prediction of Delft catamaran maneuvering in calm water and regular waves. December. In: Proc. 12th International Conference on Fast Sea Transportation. FAST, Amsterdam, The Netherlands, pp. 2–5, 2013.
- Sadat-Hosseini, H., Kim, D.-H., Toxopeus, S., Stern, F., 2015. CFD and potential flow simulations of fully appended free running 5415M in irregular waves. In: Proc. 2015 World Maritime Technology Conference, WMTC 15, Providence, Rhode Island, USA. November 3–7.
- Silverman, B.W., 1986. Density Estimation for Statistics and Data Analysis. Chapman & Hall/CRC, London.
- Stern, F., Wilson, R.V., Coleman, H.W., Paterson, E.G., 2001. Comprehensive approach to verification and validation of CFD simulations—Part 1: methodology and procedures. ASME J. Fluids Eng. 123 (4), 793–802.
- Stern, F., Wilson, R., Shao, J., 2006. Quantitative approach to V&V of CFD simulations and certification of CFD codes. *Int. J. Numer. Methods Fluids* 50, 1335–1355.
- Tahara, Y., Diez, M., Volpi, S., Chen, X., Campana, E.F., Stern, F., 2014. CFD-based multiobjective stochastic optimization of a waterjet propelled high speed ship. In: Proc. 30th Symposium on Naval Hydrodynamics. Hobart, Tasmania, Australia, pp. 2–7. November.
- Van’t Veer, R., 1998. Experimental Results of Motions, Hydrodynamic Coefficients and Wave Loads on the 372 Catamaran Model, vol. 1129. TU Delft Report.

- Van't Veer, R., 1998. Experimental Results of Motions and Structural Loads on the 372 Catamaran Model in Head and Oblique Waves, vol. 1130. TU Delft Report.
- Volpi, S., Diez, M., Gaul, N.J., Song, H., Iemma, U., Choi, K.K., Campana, E.F., Stern, F., 2015. Development and validation of a dynamic metamodel based on stochastic radial basis functions and uncertainty quantification. *Struct. Multidiscip. Optim.* 51 (2), 347–368.
- Xing, T., Stern, F., 2010. Factors of safety for Richardson extrapolation. *ASME J. Fluids Eng.* 132, 6.